LDRA

A Research Report

Final Report on

A Study of Liquid Propellant Autoignition

Contract NAS10-8591

May 1975

To
National Aeronautics and
Space Administration
Kennedy Space Center, Florida

Battelle
Pacific Northwest Laboratories

Final Report on

A Study of Liquid Propellant Autoignition

Contract NAS10-8591

May 1975

To
National Aeronautics and
Space Administration
Kennedy Space Center, Florida

Prepared by:
D. H. Lester, Principal Investigator
A. G. Gibbs
D. L. Lessor

Battelle
Pacific Northwest Laboratories
Richland, Washington 99352

ACKNOWLEDGMENTS

The authors wish to thank many NASA personnel for assistance in obtaining reference material and for discussions of past experience. Special thanks are due Mr. W. H. Boggs, NASA's Technical Representative, whose continued active interest and administrative assistance greatly contributed to this study.

We would also like to express our appreciation to Dr. Erich Farber who took time from a busy schedule to discuss his past autoignition work and also provided us with useful reference materials.

CONTENTS

1.0 SUMMARY

The purpose of this study was to review data and theory pertinent to the autoignition of liquid oxygen/liquid hydrogen (LOX/LH_2) and liquid oxygen/RP-1 (LOX/RP-1) propellants and develop, where possible, physical models of the processes supporting or contributing to autoignition. The pertinent data included that developed in a study led by Dr. Erich Farber (NASA Contract NAS 10-1255)[1] and other preceding explosive tests such as Project PYRO.[2] During the Farber study, a concept called the "Critical Mass Hypothesis" was developed which stated that when fuel and oxidizer are mixed with a certain energy, there is a mixed mass where explosion is 100% probable, called the "Critical Mass". The hypothesis is based on two simultaneous processes: 1) mixing of the propellants, and 2) development of electrostatic charge sufficient to cause ignition sparks. This is known as "autoignition". Farber's work was aimed solely at getting empirical techniques for predicting blast yield (TNT equivalents) for liquid rocket propellants. However, the objective of this study was to describe the physical environment as fully as possible and relate this description to the autoignition phenomenon.

Processes other than electrostatic charge were also explored as possible alternative or competing ignition mechanisms. Two in particular were cosmic rays and heat from ortho-parahydrogen conversion. It was found that the energy levels developed from cosmic ray ignition, while measurable, is far less than that needed to ignite an explosive hydrogen-oxygen mixture. Sufficient total energy is available in the ortho-parahydrogen conversion (from 95 to 99% para) to cause ignition, but the temperature is likely to be too low and the heat carried off easily by the surrounding fluid. Therefore, neither of these processes is considered a significant ignition mode when compared to electrostatic phenomena. External ignition sources (such as sparks from tearing metal) are not necessarily present and as such have low probability as compared with internal processes associated with autoignition by static electrical discharge.

A mixing model was developed which gave a relationship between mass which is mixed and mixing energy for energies above the boiling energy. The relationship, developed from first principles, verified the form of the high energy term in the critical mass equation.

The study of static electrical effects included three main topics. The first involved estimating the streaming potentials built up between the liquids during mixing. It was demonstrated that a sufficient electrical field for ignition, as predicted by streaming potential theory, could be built up by the relative motion of the fluids. The second was

concerned with discharge within the liquid. The dielectric breakdown within the liquid appears to be a plausible mechanism for ignition since discharge across a 0.06-cm space through a stoichiometric mixture would be a reasonable ignition source. The third considered build-up and discharge at the surface and the speculation concerning probability of ignition at the surface of the liquid mixture. It is plausible that droplet charging and droplet-droplet discharge at the surface could cause autoignition. In all these topics specific numbers could not be developed, but parameter range applicable to the cases studied were of the order of magnitude such that electrostatic discharge was reasonably probable. Further work dealing with these topics could be useful in establishing some specific estimates of discharge magnitudes.

An attempt was made to develop a model of bubble evolution to be used in conjunction with ignition and charging theories. Some basic relationships giving bubble evolution and movement were developed, although time and scope of the study did not allow investigators to completely develop a means of predicting bubble size and velocity. However, future work in this area would help relate bubble evolution to droplet and bubble charging since it appears that breakage of bubbles emerging from the surface is a contributing process to static charge build-up.

In conclusion, there are a number of processes that contribute to autoignition which appear probable. However, since some of the processes cannot be adequately described with the information at hand, much speculation results. The high energy portion of the critical mass curve comes from theory as well as experimentation which makes it quite believable. The constants in the equation depend on empirical results and more definitive experiments would be desirable. However, experience in many tests conducted by Farber indicate that the constants in the equation are substantially correct.

2.0 INTRODUCTION

This study was concerned with the explosion and fire from propellant tankage ruptures. Such ruptures can be due to equipment failure or deliberate action in testing objects to obtain blast yield parameter prediction models for safety studies. The ignition phenomena, wherein the studied fuel and oxidizer spontaneously detonate, has been called "autoignition". The yields observed in the tests indicated that little fuel and oxidizer mixing occurred at the time of ignition. One proposed mechanism for ignition at low mixed mass is a spark discharge caused by an electrostatic charge which builds up as a result of relative fluid motion between fuel and oxidizer.

2.1 BACKGROUND

An extensive experimental program, which preceded this study, was carried out under the direction of Dr. Farber. Small- and large-scale tests were carried out with propellants and many supporting experiments were conducted to gain further understanding of the mixing and ignition mechanisms; some theoretical development also accompanied the testing. The results of the experimental studies are detailed in numerous reports and summarized in the final report.[1] Farber approached the interpretation of the data from two basic directions: physical models and statistical models. The physical models led to the Critical Mass Hypothesis (as discussed below) while the statistical models were helpful in correlating predictions of explosive yields under various conditions.

The Critical Mass Hypothesis is based on the understanding gained in separate experiments on electrostatic build-up and mixing. Stated simply, the Critical Mass Hypothesis says that if the two specimens are mixed with a specific mixing energy, then a mixed mass will be reached at which 100% ignition is probable. In other words, each mixing energy has a specific critical mass. The energy released by the boiling of one species is associated with a critical mass of about 2300 lb or less. All observed explosions should fall on or below the critical mass line. It was observed that the S-IVB[3] test failure fell just below the critical mass line indicating the relationship of Critical Mass Hypothesis to failures in actual vehicle configurations.

The Critical Mass Hypothesis is based on the idea that the relative motion of the two fluids, which results from the mixing energy, causes a build-up of a static charge field. This field discharges, causing sparks that are sufficient to ignite the mixture. Other ignition sources may be present so that the mixture ignites masses that are well below the critical mass (as is often observed). No explosion occurs above the critical mass since the certainty of autoignition is 100% at the point when the critical mass of materials has been mixed.

The reality of the presence of static charge build-up was demonstrated in Farber's work by the observation of static charge in the fluids during mixing. Metal screens placed in containers registered measurable potential build-up when propellant constituents were dumped together.[4]

While the concept of autoignition appears to be experimental fact, it remains desirable to understand the physical basis for the phenomena from the standpoint of first principles.

2.2 OBJECTIVES OF THIS STUDY

The main objective of this study was to construct a theoretical basis for previously observed autoignition phenomena in LOX/LH_2 and LOX/RP-1 to whatever extent feasible within the program scope. Theoretical models of competing processes (for ignition and charge build-up) were developed to attain the objective. The most probable mechanisms for autoignition were identified and described in detail. However, development of statistical models for explosion probability and yield were not within the scope of this study.

2.3 SUMMARY OF APPROACH

The study was carried out in four basic areas (with considerable overlap between phases). In the first area, the "physical" environment* was described as much as possible. The process of bubble formation, movement and break-up was modeled as well as the process of solid formation and interstage mixing. In the second area, the static charge build-up and its relationship to requirements for detonation was described from theoretical principles. Other detonation sources (besides electrostatic) were considered in the third area and their importance, relative to the electrostatic mechanism, was considered. It is important to stress that so-called "external" ignition sources (such as those rising from metal-metal sparks) are not considered in autoignition, since such sources are not necessarily present. If these sources are present they will cause detonation at lower mixed volumes than does autoignition, thus giving yields below those predicted by autoignition (as has often been observed). In the fourth area, an attempt was made to bring all the items from the first three areas together to explain the critical mass curve or provide an adequate substitute.

---

* In this report "physical" environment refers to the various states of the fluids that are involved and the dynamics of intermixing.

3.0 THE PHYSICAL ENVIRONMENT

The physical environment governs the mixing and ignition processes. This section describes three aspects of the environment that are pertinent to autoignition phenomena: 1) the formation of vapor bubbles as the warmer fluid causes the cold fluid to boil, 2) the physics of mixing the two components with a given energy, and 3) the evolution of solid particles as one fluid freezes.

Bubbles are particularly important since they probably contribute an essential function to charge distribution and localization of discharges. Also, bubbles may be responsible for the vertical charge distribution Farber observed with his instruments.

The Critical Mass Hypothesis is directly related to the dynamics of fluid mixing. Fluid mixing and electrostatic charge build-up are interrelated in the formulation of the concept of a critical mass.

Solid particles of oxygen may be the source of oxidizer in the liquid hydrogen plug. Hydrogen bubbles associated with oxygen crystals could be the detonation mixture in LOX/LH_2 systems.

3.1 BUBBLE POPULATION DYNAMICS

Bubble population dynamics involves a description of the bubble population in a mass of boiling liquid (e.g., the H_2 plug falling into O_2). The formation, movement, and disappearance of bubbles is described.

The details of the model development can be found in Appendix A. A general model is described and some pertinent simplified cases are further developed. The models are summarized in this section.

3.1.1 The General Model

The general model includes five basic processes:

- Bubble production by nucleate boiling
- Bubble flow into and out of a region
- Bubble growth into and out of a size range
- Bubble break-up
- Coalescence of two or more bubbles

The general expression which includes all these factors is:

$$\frac{\partial n}{\partial t} + G(R)\,\frac{\partial n}{\partial R} + B(R)n = -\nabla \cdot \underline{j} + s(\underline{r},t)f(R) + \int_R^\infty n(R')B(R' \rightarrow R)dr'$$

$$+ \int_0^R \int_0^R n(R')n(R'')C(R',R'' \rightarrow R)dR'dR''$$

$$- n(R) \int_0^\infty n(R')C(R,R')dR'. \qquad (3\text{-}1)$$

where $\underline{j}$ = the flow of bubbles (bubble current)

s = nucleation probability

$f(R)$ = nucleation size distribution

B = break-up probability

C = coalescence probability

G = growth probability

While this expression includes a general description of all important phenomena it does not, in general, provide a convenient means of solving for n other than by involved numerical analysis. Specific restrictions governing the behavior of the system must be introduced to obtain usable models.

3.1.2 Some Simplifications

When applying the general equation to specific cases, more concrete statements must be made about specific gravity. Frequency functions must be determined for nucleation, coalescence and break-up; the relationship between bubble velocity, size and position must be defined; the relationship for bubble growth rate as a function of size and position must be developed; and models for discontinuous regions must be matched up. The task is clearly formidable for general models especially in obtaining solutions to the equations. However, some cases are reasonably tractable and provide some insight into the bubble population in the mixing propellants. This, in turn can be related to charge build-up and discharge across or among bubbles.

A simplification, common to all the specific models, is the neglect of bubble coalescence and break-up. This is reasonable if the bubble density is low and no very large bubbles exist. A further simplification occurs if the bubble velocity depends only on size. In this case, since there is only one growth function for all regions, it is now possible to write the current $\underline{j}$ as

$$\underline{j} = n\,\underline{V}(R).$$

The expression for j(R) can be inserted into Equation 3-1, and with the coalescence and breakup terms ignored, the result is

$$\frac{\partial n}{\partial t} + G(R)\,\frac{\partial n}{\partial R} + \underline{V}(R) \cdot \nabla n = s(r,t)\, f(R). \qquad (3\text{-}2)$$

Expressions for G(R), $\underline{v}(R)$, S(r,t) and f(R) are needed to make the relationship solvable. It then becomes a first order, partial, differential equation for n(r,R,t).

3.1.3 The Two Region Model

In the case of two liquids coming into contact with one boiling, the general equation must be applied to two regions: one where bubble evolution and growth occurs in a boundary layer under a supersaturated condition, and one where the surrounding liquid is saturated but not superheated.

The Boundary Region

The growth in the boundary region can be described from empirical relationships in the literature (see Appendix A). The radius of the bubble as a function of time is

$$R = \left[\left(\frac{12}{\pi}\right)^{1/2} \frac{K}{\rho_v Q a^{1/2}}\right] \zeta_o\, t^{1/2} \qquad (3\text{-}3)$$

where K = conductivity

ρ_v = vapor density

Q = latent heat

a = thermal diffusivity

ζ_o = superheat

t = time

Therefore

$$R = \overline{K}\, t^{1/2},\ \overline{K} = \text{constant}$$

A force balance on the individual bubble provides an equation of motion on the assumption that the chief impetus for bubble motion in the boundary region is buoyancy:

$$\text{Net Force} = \text{Buoyancy} - \text{Drag}$$

$$\frac{4}{3}\pi R^3 \rho_b \frac{dV}{dt} = \frac{4}{3}\pi R^3 \rho g - 6\pi\mu RV. \quad (3\text{-}4)$$

The problem becomes one-dimensional in the vertical direction so that $\underline{r}$ becomes Z. Rearranging Equation (3-4) gives

$$\frac{dV}{dt} + \frac{9\mu}{2\rho_b R^2} V = \frac{\rho g}{\rho_b}$$

From the growth equation (Equation 3-3)

$$\frac{dV}{dt} = \frac{dV}{dR}\frac{dR}{dt} = \frac{dV}{dR}\left(\frac{\overline{K}^2}{2R}\right). \quad (3\text{-}5)$$

Equation (3-5) can be solved for V(R) so that

$$V(R) = \left(\frac{C_2}{C_1 + 2}\right) R^2 \quad (3\text{-}6)$$

where

$$C_1 = \frac{9\mu}{\rho_b \overline{K}^2} \qquad C_2 = \frac{2\rho g}{\overline{K}^2 \rho_b}$$

therefore

$$\frac{dZ}{dt} = V(R) = \left(\frac{C_2 \overline{K}^2}{C_1 + 2}\right) t \quad (3\text{-}7)$$

and

$$Z = Z_o + \left(\frac{C_2 \overline{K}^2}{2(C_1 + 2)}\right) t^2 \quad (3\text{-}8)$$

In one dimension, Equation (3-2) becomes

$$\frac{\partial n}{\partial t} = G(R)\frac{\partial n}{\partial R} + V(R)\frac{\partial n}{\partial z} = S(z,t)\, f(R) \quad (3\text{-}9)$$

where

$$G(R) = \frac{dR}{dt} = \frac{\overline{K}^2}{2R}$$

$$V(R) = \left(\frac{C_2}{C_1 + 2}\right) R^2$$

If we assume that nucleation proceeds at a constant rate and a single size then

$$f(R) = \delta(R) \qquad \text{dirac delta function}$$

and

$$S(z,t) = S = \text{constant rate of nucleation}$$

Equation (3-9) can be solved to give

$$n(z,R,t) = \frac{S}{\sqrt{Az}}\,\delta\left[R - \overline{K}\left(\frac{z}{A}\right)^{1/4}\right] H\left[t - \left(\frac{z}{A}\right)^{1/2}\right] \qquad (3\text{-}10)$$

where

$$H(t) = \begin{cases} 1 & t > 0 \\ 0 & t < 0 \end{cases}$$

$$A = \frac{C_2\overline{K}^2}{2(C_1 + 2)}\,.$$

At the interface where Z = h

$$n(h,R,t) = \frac{S}{\sqrt{Ah}}\,\delta\left[R - \overline{K}\left(\frac{h}{A}\right)^{1/4}\right] H\left[t - \left(\frac{h}{A}\right)^{1/2}\right]. \qquad (3\text{-}11)$$

For example, if the degree of superheat is 5°C (the real value will be greater than zero and less than 20°C) in liquid hydrogen then

$$\overline{K} = 0.068 \ \text{m/sec}^{1/2}$$

and

$$C_1 = 3.89$$

$$C_2 = 2.97 \times 10^4 \quad (m/sec)^{-1}$$

$$A = 1.04 \times 10^5 \quad m/sec.$$

Then a 0.25-in. bubble (such as observed by Farber) will emerge from a boundary region of thickness

$$h = \left[\frac{RA^{1/4}}{\overline{K}}\right]^4 = 7.9 \text{ cm.}$$

Furthermore, if $S = 1 \times 10^6$ nuclei/sec-m^3 at $z = 0$ (an arbitrary guess) then

$$n = 1.1 \times 10^5 \quad \frac{0.25 \text{ in. bubbles}}{\text{sec} - m^3}$$

at the interface.

The Bulk Fluid

The following set of equations describes the bulk fluid for the simplified case to be considered. Detailed arguments developing these equations can be found in Appendix A.

$$\frac{dM}{dt} = 0 \text{ (no mass transfer)}$$

$$\frac{ds}{dt} = 0 \text{ (constant total entropy)}$$

$$\rho_v(z) = \frac{P(z)}{r\,T(z)} \text{ (vapor is ideal gas)}$$

where r = gas law constant

$$S_v(z) = C_{pv} \ln \frac{T}{T_1} - r \ln \frac{P}{P_1} \text{ (vapor entropy)}$$

T_1, P_1 reference state

ρ_L = constant liquid density

$$S_L(z) = C_{PL} \ln \left(\frac{T}{T_2}\right)$$

T_2 Reference State

$$P(z) = P_o - \rho_L g z \quad \text{(hydrostatic pressure)}$$

These equations are manipulated (in Appendix A) to get the density of a bubble

$$\rho(z) = \frac{\rho_v(z)\, Q}{T(z) \left(1 - \frac{\rho_v(z)}{\rho_L(z)}\right) \left[C_{PV} \ln \frac{T_o}{T_1} - r \ln \frac{P_o}{P_1} - C_{PL} \ln \frac{T}{T_2}\right]} \quad (3\text{-}12)$$

where Q = latent heat

$$\rho_v(z) = \frac{P_o - \rho_L g z}{r\, T(z)}$$

$T(z)$ = saturation temperature at $P(z)$

T_o, P_o = T, P at z = 0

Since $\frac{dM}{dt} = 0$, then $M = M_o$ so that

$$R(z) = \left[\frac{3M_o}{4\pi\, \rho(z)}\right]^{1/3}.$$

With similar arguments for buoyancy forces as in the boundary region development

$$V \frac{dV}{dz} = - \frac{6\pi\, \mu\, R(z)}{M_o} V + \left(\frac{\rho_L - 1}{\rho(z)}\right) g$$

or

$$\frac{dV}{dz} = \frac{h(z)}{V} - f(z). \quad (3\text{-}13)$$

where

$$h(z) = \left(\frac{P_L}{\rho(z)} - 1\right) g \quad \text{and} \quad f(z) = \frac{6\pi \mu R(z)}{M_o}$$

and velocity can be obtained from

$$V(z) = V_o - \int_0^z f(z')\, dz' + \int_0^z \frac{h(z')}{v(z')}\, dz' \qquad (3\text{-}14)$$

which must be solved numerically since it does not have a closed-form solution. After numerical integration R(z), V(z) and, therefore, V(R) are known and

$$\frac{\partial n}{\partial t} + F(z) \frac{\partial n}{\partial R} + V(R) \frac{\partial n}{\partial z} = 0 \qquad (3\text{-}15)$$

where

$$\frac{dR}{dt} = \frac{dR}{dz}\frac{dz}{dt} = V(z) \frac{d}{dz} \left[\left(\frac{3M_o}{4\pi\, p(z)}\right)^{1/3}\right] = F(z).$$

Equation (3-15) could then be solved numerically to obtain n(z,R,t) in the bubble fluid. The boundary condition for the solution would be n(h,R,t) obtained from Equation (3-11).

3.2 THE SOLID OXYGEN PHASE

In the hydrogen-oxygen case there is a large temperature difference between the two components. If the tanks are at atmospheric pressure, the hydrogen will be at 20°K and the oxygen at 90°K. The oxygen will tend to boil hydrogen and at the same time will cool rapidly. Since the melting point of oxygen is 55°K, which is well above the hydrogen temperature, it is likely that solid oxygen will form.

The heat removed by hydrogen/vaporization is related to oxygen cooling and freezing by

$$M_H \lambda_H = M_o' C_o (T_o^B - T_o^M) + M_o \lambda_o + M_o'' (\Delta T)$$

where

M_H = mass of H_2 vaporized,

M_o = mass of O_2 frozen,

M_o' = mass of O_2 cooled from T_o^B to T_o^M,

C_o = heat capacity of oxygen,

M_o'' = mass of O_2 cooled some other amount ΔT,

ΔT = arbitrary temperature difference (unknown),

λ_H = latent heat of vaporization of hydrogen,

λ_o = latent heat of fusion of oxygen,

T_o^B = boiling point of oxygen, and

T_o^M = melting point of oxygen.

The largest crystal mass of oxygen will be formed when all heat used to boil hydrogen is taken from a certain mass of oxygen which is subsequently frozen (that is $M_o = M_o'$, $M_o'' = 0$ in the heat balance).

Therefore, the largest crystal occurs when

$$M_H \lambda_H = M_o C_o (T_o^B - T_o^M) + M_o \lambda_o$$

$$\text{then } \frac{M_H}{M_o} = \frac{(T_o^B - T_o^M) C_o + \lambda_o}{\lambda_H}$$

$$\frac{M_H}{M_o} = \frac{35\ (0.394) + 3.3}{108}$$

$$= 0.156.$$

The volumetric ratio is

$$\frac{V_H}{V_o} = \frac{0.156\ (1.41)}{1.2 \times 10^{-3}} = 183$$

and the mole ratio is

$$\frac{\text{moles hydrogen}}{\text{moles oxygen}} = \frac{32}{2}\ (0.156) = 2.5.$$

If the hydrogen was in the form of 0.25-in. bubbles, then the associated oxygen crystal would have a volume of about 7×10^{-4} cm^3 which, if spherical, would be about 0.09 in. in diameter. Therefore, one might envision a 0.09-in. diameter oxygen crystal (or smaller) associated with each 0.25-in. hydrogen bubble.

The oxygen crystals would account for very little of the mixed hydrogen volume, but could be important if not essential to detonation. In another propellant safety study it was found that if a nitrogen-oxygen mixture of at least 75% oxygen was mixed with hydrogen, sufficient solid oxygen was formed to support detonation of the hydrogen by a spark.[5] The quantity of 75% oxygen added to 300 g hydrogen was 75 g which means that about 16% solid oxygen in the hydrogen is needed.

The system could be modeled as follows. The hydrogen mass is a plug of fluid entering the oxygen pool. As the plug enters, hydrogen bubbles and solid oxygen crystals are formed and dispersed through the hydrogen (because of the very small size of the oxygen crystals). Arcs across bubbles or from bubble to bubble must be in the presence of oxygen close to the bubbles; the essential oxygen would probably be in the form of solid crystals. Thus, it appears that one whould view the process as a spark (across bubbles or between bubbles) which vaporizes some oxygen from the solid and sets off the hydrogen-oxygen gas mixture.

3.3 MODELING OF THE MIXING PROCESS

When one liquid is released into the other, a mixing process begins. The Critical Mass Hypothesis is based on the idea that a static charge is building up simultaneously with the mixing so that a critical mass is mixed when sufficient charge is built up to guarantee ignition. The critical mass curve is based on the relationship between mass mixed and mixing energy. The shape of the curve is governed by the mass-energy relationship while the specific constants are determined from the data on charge build-up.

The mixing model described here (and detailed in Appendix B) shows that the shape of the high energy portion of the critical mass curve can be derived from first principles.

In the high energy region it is reasonable to assume that the mixing is due to isotropic turbulence. A relationship between mixing energy and quantity mixed can then be developed from Kolmogoroff theory of turbulent mixing.

The ratio of the amount of A mixed with B (= m) and the total amount of A can be described in terms of time and a constant, which depends on the power density (energy density):

$$\frac{m}{M} = 1 - e^{-t/\gamma}$$

where

$$\gamma = \frac{\rho}{6\mu} \left[\frac{\mu^{3/4}}{\rho^{1/2}}\right] \left(\frac{P}{V}\right)^{-1/4}$$

$$\frac{P}{V} = \text{power/unit volume}$$

Incegration of the relationship over a period of time with a constant influx rate dM/dt gives

$$m = k_1 t - \frac{k_1}{k_2}(1 - e^{-k_2 t})$$

where k_1, k_2 are constants.

Using the relationship for energy

$$E = Mgx$$

where x = ullage space height and expanding the m(t) relationship gives

$$m = K_5 E^2$$

where K_5 = constant

as the first term in the series. It can be shown that other terms in the series are small for conditions of interest. This term is identical with the high energy term in the critical mass equation.

Therefore, this theory developed on first principles appears to support the empirical interpretation used by Farber to develop the high energy term in the critical mass curve.

4.0 MECHANISMS OF ELECTROSTATIC IGNITION

A number of electrical ignition mechanisms can be postulated in the rapid mixing of liquid oxygen (LOX) with liquid hydrogen (LH_2) or liquid hydrocarbon fuels (like RP-1). These include:

1) electric discharge across combustible fuel-oxygen vapor mixtures within the mixture bulk,
2) liquid dielectric breakdown discharge across both fuel and oxygen within the mixture bulk, releasing a combustible vapor mix, and
3) electric discharge through combustible vapor from or among droplets ejected from the surface in boiling.

A necessary condition for any of these electrical ignition mechanisms is a charge separation giving rise to a potential difference sufficient to cause a discharge.

4.1 STREAMING POTENTIALS IN FUEL-LIQUID OXYGEN MIXING

The streaming potential phenomenon has been long known to exist in flows through capillaries and porous plugs, and a quantitative treatment has long been available although it does have restrictive assumptions.[6] The phenomenon has been described mathematically and consistency of the description has been verified experimentally[7,8] for laminar flows of fluids through capillaries and porous plugs.

This streaming potential phenomenon occurs as a consequence of the electrical double layer at the interface between two materials. The interaction of the two materials results in thin regions which are not electrically neutral in the region of the interface. Since the region of electrical charge is thin but of finite extent, some of the charge gets carried away with the liquid flow at a solid-liquid interface (or presumably at a liquid-liquid, liquid-gas, or other interface at which there is both close contact and relative motion). The convective flow of charge results in the buildup of an electric field which in steady-state drives a conductive current of equal magnitude and opposite sense to the convective current. This electric field is responsible for the streaming potential.

In the mixing of LOX and either LH_2 or hydrocarbon fuels, we picture globules, plugs, or columns of a liquid (Liquid A) plunging into another liquid (Liquid B) (and possibly bubbling back upward due to buoyancy). The convective charge flow at the interface where there is relative motion of the two materials would result in a vertical electric field, hence a potential difference between vertically separated points. This may be responsible for the potential difference measured by Farber between vertically separated screen pairs below the lower liquid surface when liquid fuels were poured into LOX and vice versa. Since bubbles of the more volatile component (hydrogen in hydrogen-oxygen mixing, oxygen

in oxygen-hydrocarbon fuel mixing) would be forming most rapidly near the interface and would possibly have a combustible admixture of the less volatile component, the electric field resulting from the convective charge flow could conceivably cause ignition by discharge across bubbles. In the following discussion we will try to estimate the electric field that could result.

Consider a plug, column, or filament of Liquid A plunging into Liquid B. Suppose Liquid A moves with velocity $\underline{v}$ and that most of Liquid B moves more slowly. The convective current i_1 through a cross section of the column is[9]

$$i_1 = \int_S \rho_q \, \underline{v} \cdot \underline{dS} \tag{4-1}$$

where the surface is a cross section of the column and ρ_q is the charge density. The charge density satisfies the Poisson equation in (Gaussian units):

$$\nabla^2 \psi = -4\pi\rho_q/\kappa. \tag{4-2}$$

If we take the charge density as resulting from the chemical interaction at the interface and maneuver Equations (4-1) and (4-2), we obtain as the dominant term

$$i_1 \simeq -\frac{\zeta\kappa}{4\pi} \oint_C \underline{dl} \cdot (\nabla x \underline{v}). \tag{4-3}$$

Here, ζ is the value of the potential ψ at the interface and is known in electrochemical and electrokinetic work as the zeta potential. The line integral in Equation (4-3) is around the edge of the surface S.

The traditional expression for streaming potential in a capillary involves the Poiseuille expression for laminar viscous flow in a cylinder. Although we do not necessarily expect laminar flow in the dumping of Liquid A into Liquid B, we do expect a boundary layer at the interface. We also expect the curl of the velocity at the surface to be

$$\nabla x \underline{v} \simeq \frac{v}{\delta} \hat{t} \tag{4-4}$$

where scaler v = velocity at the center of the column, δ = the thickness of the boundary layer, and $\hat{t}$ = a unit vector tangential to the boundary, c, of the surface, s. Accordingly, the convective current i_1 is

$$i_1 = \frac{-\zeta\kappa \frac{v}{\delta} l_c}{4\pi} \tag{4-5}$$

where l_c = the length of the perimeter of the flowing column of fluid.

The convective flow of charge results in a charge separation and hence in an electric field that tries to restore charge neutrality by conduction. The return conductive flow path could be through both the column of Liquid A or through Liquid B. To see what electric field magnitudes might result, consider the case where Liquid B is of much lower electrical conductivity than Liquid A. If the flow continues long enough, a conductive current i_2 will build up so to give a zero total current:

$$i_2 + i_1 = 0. \tag{4-6}$$

Here, conductive current i_2 is given by

$$i_2 = \int \sigma \underline{E} \cdot \underline{ds} \simeq \sigma \langle E \rangle A, \tag{4-7}$$

where σ = conductivity of Liquid A, and

A = cross sectional area of the flow stream

$\langle E \rangle$ = average electrical field across flow stream.

From Equations (4-5) through (4-7) we deduce an electric field magnitude

$$\langle E \rangle \simeq \frac{\zeta v l_c \kappa}{\sigma A \delta 4\pi} \tag{4-8}$$

This approximate relation is useful for estimating the electric field which might develop, although the average electric field could differ substantially from the peak value for large area flow columns. For large area flow columns, the conductive flow and the electric field driving it might be limited to regions near the interface.

Dimensional arguments give a boundary layer thickness on the order of

$$\sigma \simeq \left(\frac{\mu x}{\rho_m v}\right)^{1/2} \qquad (4\text{-}9)$$

where μ = coefficient of viscosity,

ρ_m = mass density,

v = velocity at points away from the interface, and

x = distance from leading edge of the surface along which the boundary layer develops.[10]

For our picture of a column of Liquid A penetrating into Liquid B, distance x is the distance from the leading end of the column. However, Expression 4-9 for the boundary layer thickness should not be taken too seriously for x approaching zero nor for δ larger than the order of one-fourth of the transverse flow dimensions, the latter being the laminar flow limit.

We insert Equation (4-9) into Equation (4-8) for a circular cylindrical column and substitute plausible values for hydrogen plunging into oxygen:

v = 600 cm/sec (velocity of the plug)

ζ = 0.1 volt = 0.333×10^{-3} statvolt (estimated zeta potential, uncertain by factor $\sim$3 and sign)

r_c = 3 cm (radius of column)

x = 5 cm (distance from end of column)

μ = 1.4×10^{-4} gm/cm sec (LH_2 viscosity at boiling point, 20°K)

κ = 1.23 (dielectric constant)

$(1/\sigma)$ = 10^{17} ohm cm = $1/9 \times 10^{6}$ sec (resistivity of liquid hydrogen)*

ρ_m = 7.1×10^{-2} gm/cm^3 (liquid hydrogen density).

The estimated electric field with this set of numbers in Equations (4-8) and (4-9) is

$$\langle E \rangle = -3.6 \times 10^{5} \text{ statvolt/cm} = -1.07 \times 10^{8} \text{ volt/cm}.$$

---

* The estimated hydrogen resistivity is uncertain by orders of magnitude due to ionic impurity content. The number used was reported by Cassutt[11] = 10^{17} ohm cm.

Using an electric resistivity 4 orders of magnitude lower would give $\langle E \rangle = 1.07 \times 10^5$ volt/cm, which is still a plausible number

The breakdown fields in hydrogen gas at atmospheric pressure and 20°K are $\sim 1 \times 10^5$ volts/cm. Thus, breakdown field strengths could conceivably be greatly exceeded by the streaming potential mechanism, but sharpening of both the model and the physical parameters is needed.

One interesting property of streaming potentials is that the zeta potential, ζ, can be markedly affected by impurities in the liquid. For example, the effect on the zeta potential of adding $Th(NO_3)_4$ to water (shown in Table 4-1) is appreciable for very small quantities of solute.[12] In fact, the sign of the zeta potential can actually be changed by impurities. This leads to the speculation that reversed polarities in Farber's voltage measurements could have been due to build-up of impurities in the test system.

TABLE 4-1. Effect of Th $(NO_3)_4$ on Zeta Potential Between Water and Glass

Zeta Potential (volts)	Concentration of $Th(NO_3)_4$ in Water (ppm)
-0.16	0
0	48
+0.14	4800

Marked changes in resistivity and the zeta potential itself could greatly alter the charge build-up rates. However, it is not certain what kind of impurities one might find in liquid hydrogen or oxygen. By the nature of their cold temperatures, the cryogenic liquids resist dissolution of most impurities.

4.2 DISCHARGE ACROSS VAPOR BUBBLES IN THE LIQUID

Dielectric breakdown within the liquid is plausible for ignition. However, it requires not only an electric field which is sufficient to cause breakdown, but also requires dissipation of enough energy to vaporize material in a region of transverse dimensions which are larger than the quenching distance (quenching distance is smallest distance from a wall or other structure for which a combustion process can continue). Walls or liquid materials can "quench" combustion in vapors by robbing either heat or reacting ions. The quenching distances for various concentrations of hydrogen in air are given in Table 4-2.[13] A spacing of 0.06 cm is required for stoichiometric properties with much larger spacings (approaching 1 cm) for high or low hydrogen percentages; hydrocarbons (like RP-1) would require even greater distances. We anticipate somewhat

shorter quenching distances for dielectric surfaces like LOX or LH_2 than these experimental values measured with metal electrodes, but of the same order. See Appendix C for discussion.

TABLE 4-2. Parallel Plate Quenching Distances for Hydrogen-Air Mixtures

H_2 by Volume, %	Quenching Distance, cm
5	0.60
10	0.15
30	0.06
60	0.20
70	0.60

Liquid dielectric breakdown ignition might result from discharges terminating on oxygen crystals in LOX-LH_2 mixing or on wax-state hydrocarbon fuels in LOX-liquid hydrocarbon mixing. Further discussion of oxygen crystals appears in Section 3.1 under "The Solid Oxygen Phase".

The contact potential mechanism gives rise to a finite thickness charge layer at the interface between materials, as will be discussed further in Section 4.3. Rising bubbles of hydrogen vapor will have a tendency to have part of the charge outside them sheared off by the relative motion as shown in Figure 4-1. The charge separation results in a vertical field component which tends to pull the external charge along with the bubbles. This vertical electric field component could contribute to the potential difference observed by Farber between vertically separated horizontal screens.

The charge in the liquid just outside a bubble surface is approximately

$$Q_B = 4\pi r^2 Q_A$$

where Q_A is charge per unit area. Relative motion of bubble and liquid attempts to sweep this charge off, resulting in an average convective current J_C in the liquid from a dense cloud of moving bubbles given by

$$J_c = n_v V_{eff} Q_B$$

where V_{eff} is the effective (for carrying charge) flow velocity component in the mean flow direction. Here n_v is number of bubbles per unit volume. The value of effective velocity V_{eff} is less than the relative velocity of fluid to bubbles, because of boundary layer effects. It is a function of both charge layer thickness and flow boundary layer thickness. An electric field develops which tends to keep the charge moving

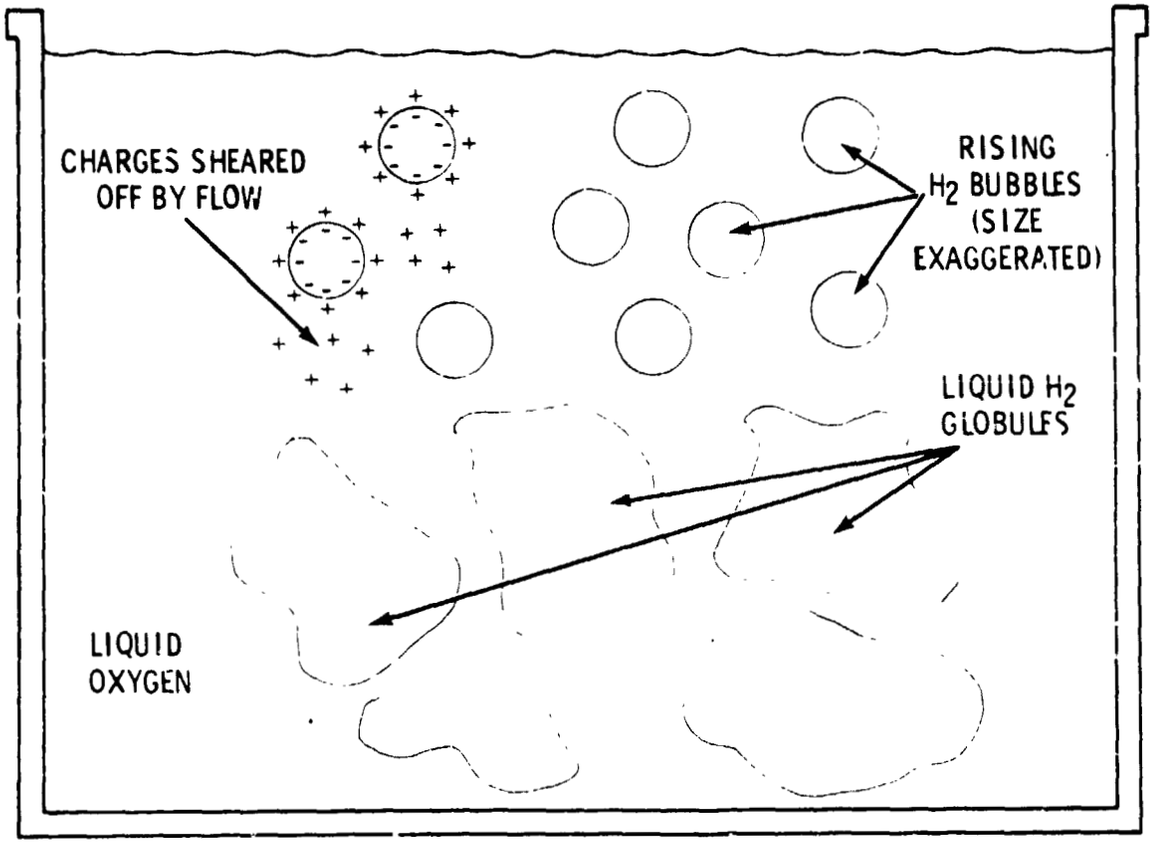

FIGURE 4-1. Rising Bubble Charge Transport

with the bubbles. Equating this conductive current magnitude to that of the oppositely directed convective current gives

$$\sigma \langle E \rangle = n_v V_{eff} Q_B$$

This can be written

$$\langle E \rangle = \frac{1}{\sigma} V_{eff} n_v 4\pi r^2 Q_A$$

$$= \frac{1}{\sigma} V_{eff} \beta \frac{3}{r} Q_A$$

where $\beta = (4/3)\pi r^3 n_v$ is the volume fraction occupied by bubbles.

To develop an order of magnitude estimate of $\langle E \rangle$, observe that effective velocity V_{eff} is likely to be given by something like

$$V_{eff} \sim V_{av} \cdot \frac{s}{\delta}$$

where V_{av} is average relative velocity of fluid to bubbles, s is charge layer thickness, and δ is fluid boundary layer thickness. We assume $s < \delta$. We will take as an approximation for Q_A (in cgs Gaussian units)

$$Q_A \simeq \frac{\varepsilon}{4\pi} \frac{V_o}{s}$$

Where V_o is a potential at the interface that is on the order of the difference in work functions for the two materials and ε is relative dielectric constant. These approximations give

$$\langle E \rangle \sim \frac{1}{\sigma} \beta V_{av} \frac{3\varepsilon}{4\pi} \frac{V_o}{r\delta}$$

We further take the average relative velocity V_{av} to be the Stokes velocity (valid only for small bubbles),

$$V_{av} = \frac{2}{9} \frac{r^2}{\eta} (\rho_L - \rho_B)\, g,$$

where η is fluid viscosity, ρ_L and ρ_B are liquid and bubble densities, and g is the acceleration of gravity. With this V_{av} we obtain

$$\langle E \rangle = \frac{\varepsilon}{6\pi} \frac{\beta}{\sigma} \frac{r}{\delta} \frac{(\rho_L - \rho_B)\, g}{\eta} V_o$$

Inserting arbitrary but plausible parameters,

$\sigma = 0.009 \text{ sec}^{-1} = 10^{-14} \text{ (ohm cm)}^{-1}$

$\beta = 0.1$

$\varepsilon = 1.46$

$(r/\delta) = 10.$

$\rho_L = 1.14 \text{ gm/cm}^3$

$\rho_B = \text{negligible}$

$g = 980 \text{ cm/sec}^2$

$V_o = \frac{0.1}{300}$ statvolt = 0.1 volt

$\eta = 9 \times 10^{-3} \text{ gm (cm-sec)}^{-1}$

we obtain

$$\langle E \rangle = 3.6 \times 10^2 \text{ statvolts/cm} = 1.1 \times 10^5 \text{ volts/cm}$$

This field strength compares with a dielectric breakdown field of 10^5 volt/cm in 20°K hydrogen gas. This suggests that discharge across rising hydrogen bubbles is possible by this mechanism.

4.3 ELECTROSTATIC CHARGING EFFECTS AT SURFACES OF MIXING LIQUIDS

If two liquids whose vapors from combustible mixtures are violently mixed (as by dumping one into the other), the cover gas-liquid interface seems a likely place for ignition. For volatile materials, a combustible mixture at many locations over the surface is probable. One is therefore led to seek a mechanism for electrical discharge of sufficient intensity for ignition at the surface.

Experimental work of Harper[14] verified charging of liquid droplets formed at a number of liquid surfaces. His data was obtained by bubbling nitrogen gas up through the liquids. Charged droplets of both signs were seen (though not in equal numbers) when froth bubbles broke. While the exact mechanism for this charging cannot be deduced from these experiments, the experiments do seem to prove that droplets charging so formed does occur. We believe that contact potential mechanism is responsible for the charging observed by Harper. If an electric field is present, an induction process can also contribute to droplet charging. Harper, however, attributed his droplet charging to shear in electrical double layers.

Qualitatively, a space charge layer is known to occur near the interface between dissimilar materials. The space charge region supplies the electrical potential difference needed to give zero net current at equilibrium between dissimilar materials in contact. Treating the case of metal-semiconductor contacts, Schottky proposed a model in which the width of this space charge region is proportional to the square root of the contact potential and inversely proportional to the square root of the number density of donor (acceptor) atoms for an n (p) type semiconductor. If this qualitative dependence on donor atom density holds, then the space charge region becomes thick for highly resistive, very pure cryogenic liquids. A thick region of space charge in the liquid oxygen around a hydrogen bubble when it breaks the surface gives an opportunity for charged oxygen droplet formation. Presumably there would be opposite sign charging on high mobility hydrogen molecules.

This postulated liquid oxygen droplet charging at the surface of the LOX-hydrogen mixture could conceivably lead to ignition in a number of ways:

1) Electrical discharge between an oxygen droplet and the bulk liquid as the droplet is ejected away in froth bubble breakage,

2) Electrical discharge between a charged droplet and the bulk liquid as the charged droplet falls back into the liquid,

3) Discharge between flying droplets with dissimilar levels of charging,

4) Miniature "lightning" flashes if cover gas flow over the surface or difference in mobilities separates charged oxygen droplets from oppositely charged hydrogen gas,

5) Droplet-droplet discharge by the following sequence of events: Cover gas flow over the LOX-hydrogen mix, difference in mobilities, or gravitational effects separate oxygen droplets from oppositely charged hydrogen gas. Droplets formed under the non-space-charge-neutralized oxygen droplet cloud get opposite sign charge by induction. Droplets of opposite sign spark discharge in passing.

A sketch showing droplet charging at the liquid surface is shown in Figure 4-2.

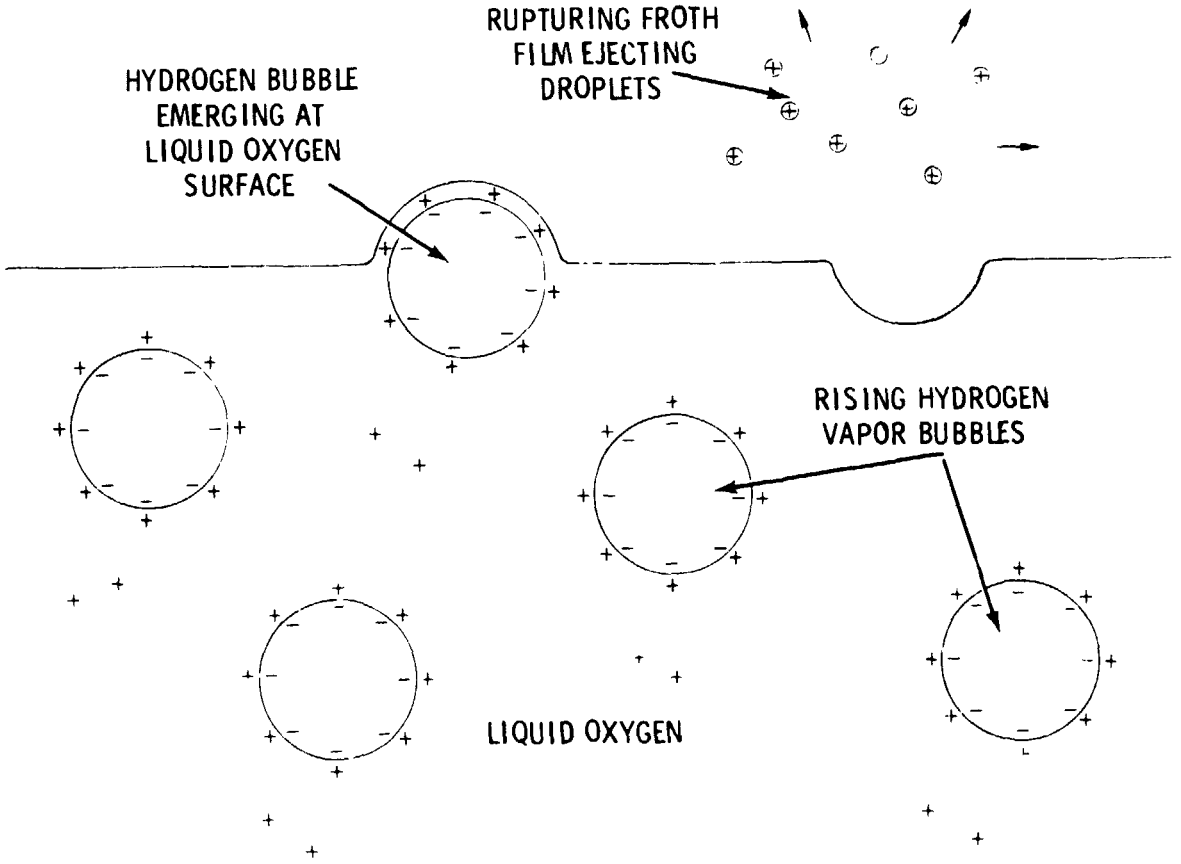

FIGURE 4-2. Surface Froth Droplet Charging Effects

For mixing LOX and RP-1, similar postulates may still explain surface autoignition. Oxygen vapor bubbles rise rapidly to the surface with contact potential charge distributions in the RP-1 layers around it and in the oxygen vapor of the bubble. The RP-1 droplets get a charge when the froth breaks at the surface. Some of the RP-1 around a rising oxygen bubble may be wax, just as some of the oxygen around a rising hydrogen bubble may be crystalline.

It should be noted that in the autoignition work of E. A. Farber et al., the ignition source location in Figure 80 of Reference 1, suggests a surface ignition phenomenon.

4.3.1 Contact Potential Effects in Cryogenic Fluid Mixing

The conduction mechanism in liquid hydrogen and liquid oxygen probably involves impurities, but it is not clear (to this writer) whether the charge carriers are ions or electrons or holes. We favor electrons or holes as the contributors, since ion mobility should be low at cryogenic temperatures. Also, at cryogenic temperatures it seems likely that there is a fair amount of spatial order of molecules, i.e., on a scale of several to several hundred intermolecular distances. Hence, it seems appropriate to use the terminology and models of solid state semiconductor physics to these liquids (e.g., conduction and valence bands, conduction band electrons and valence band holes, donor and acceptor impurities, etc). At the same time, it seems appropriate to regard conduction band electron wave functions (if this is a valid concept) as localized over a distance on the order of the molecular order range. Thus, it is appropriate to speak of a spatial variation of electron number density on distances of this order; we emphasize that these conjectures are (at least to us) speculative.

The high resistivity of cryogenic liquid hydrogen[11] of high purity suggests that the number density of charge carriers is very low. If conduction is by electrons or holes, the resistivity should be extremely sensitive to donor or acceptor impurities, because the number density of intrinsic charge carriers is so low. Measurements of L. Cassutt, et al.,[11] showed insensitivity of resistivity to air or nitrogen impurities, which suggests only that the air or nitrogen impurities were not good donors or acceptors in liquid hydrogen, i.e., they did not ionize. We did not uncover corresponding information for liquid oxygen.

The charge density near the interface needed to produce the electrostatic potential difference obeys Poisson's equation (written here in cgs Gaussian units):

$$\nabla^2 V = -\frac{4\pi\rho}{\varepsilon} \tag{4-10}$$

$$= -\frac{4\pi}{\varepsilon}\sum_i q_i n_{io} e^{-\frac{q_i V}{kT}} . \tag{4-11}$$

Here, the assumed spatial dependence of the number density n_i of charges of species i is given by:

$$n_i(\underline{r}) = n_{io}\, e^{-\frac{q_i V(\underline{r})}{kT}}, \tag{4-12}$$

where V is electrostatic potential, q_i is charge per particle of species i, T is absolute temperature, and ε is the dielectric constant of the medium. This relationship can be considered a classical Boltzmann statistical dependence for ions or as a low concentration limit for electrons and donors or holes and acceptors, as we shall discuss later. To see the nature of the charge distribution near the interface, it will be sufficient to consider the region $x > 0$ when the interface is at $x = 0$ and to assume that for x large, V, ρ, and dV/dx approach zero. With only an x dependence of electrostatic potential, V, and these assumptions, Equation (4-11) yields a first integral

$$\left(\frac{dV}{dx}\right)^2 = \frac{8\pi kT}{\varepsilon} \sum_i n_{io} \left[\exp\left(-\frac{q_i V}{kT}\right) - 1\right]. \tag{4-13}$$

If we take only two charge species of positive charge q and negative charge -q and take the positive x side as medium 2 when $V_1 - V_2 > 0$ (so $dV/dx < 0$), then Equation (4-13) gives

$$\frac{dV}{dx} = -\left(\frac{8\pi kT n_o}{\varepsilon}\right)^{1/2} \left(e^{\frac{qV}{2kT}} - e^{-\frac{qV}{2kT}}\right) \tag{4-14}$$

where n_o is the number density of either sign charge at large x. Separation of variables in Equation (4-14) and integration yields

$$\log \frac{[\exp(qV/kT) + 1][\exp(qV_o/kT) - 1]}{[\exp(qV/kT) - 1][\exp(qV_o/kT) + 1]} = \kappa x \tag{4-15}$$

where

$$\kappa = \left(\frac{8\pi q^2 n_o}{\varepsilon kT}\right)^{1/2}. \tag{4-16}$$

Here, V_o is the value of V at the plane of the interface.

Similar treatment of the other side of the interface gives

$$\log \frac{[\exp(q\tilde{V}/kT) - 1][\exp(q\tilde{V}_0/kT) - 1]}{[\exp(q\tilde{V}/kT) - 1][\exp(q\tilde{V}_0/kT) + 1]} = -\kappa x \tag{4-17}$$

where

$$\tilde{V} = V - (V_1 - V_2)$$

$$\tilde{V}_0 = \tilde{V}\ (x = 0)$$

$$\kappa = \left(\frac{8\pi q^2 \tilde{n}_0}{\tilde{\varepsilon} kT}\right)^{1/2} \tag{4-18}$$

$\tilde{n}_0$ = Number density of current carriers for $X \ll 0$

$\tilde{\varepsilon}$ = Dielectric constant for $x < 0$.

Note that $V_1 - V_2$ will be determined at equilibrium by Equation (D-5) in Appendix D, "Contact Potential Fundamentals" and will be essentially a work function difference. V_0 will be between zero and $V_1 - V_2$, and can be calculated by requiring continuity of dV/dx across the interface.

The space charge region will be of thickness

$$S_2 = (\kappa)^{-1} = \left(\frac{\varepsilon kT}{8\pi q^2 n_0}\right)^{1/2} \tag{4-19}$$

in Medium 1 ($x > 0$) and of thickness

$$S_1 = (\tilde{\kappa})^{-1} \tag{4-20}$$

in Medium 1. To understand this, consider the case $V \ll kT$. Then Equation (4-15) gives

$$V(x) = V_0\, e^{-\kappa x}\ . \tag{4-21}$$

A graph of qV/kT versus κx according to Equation (4-17) for several values of qV_o/kT can be found in H. R. Kruyt, Reference 9.

Note that Equation (4-19) implies thick space charge boundary layers for interfaces at a low temperature in a media with a low number density of mobile current carriers. It is necessary to show that the number density of charge carriers can be sufficiently low that the space charge region can be on the order of the thickness of the liquid oxygen film when a hydrogen vapor bubble emerges at the surface. We would then expect significant charging of droplets formed when the film breaks. If the space charge region is only a few molecule separations thick, it would appear that charge separation in the film breakage would be unlikely.

We can calculate the charge per unit area in Medium 2 at the interface from

$$\sigma = \int_0^\infty \rho dx = -\frac{\varepsilon}{4\pi}\int_0^\infty \frac{d^2V}{dx^2}\,dx \tag{4-22}$$

$$= \frac{\varepsilon}{4\pi}\left(\frac{dV}{dX}\right)_{x=o} \tag{4-23}$$

$$= -\frac{\varepsilon}{4\pi}\left(\frac{8\pi kTn_o}{\varepsilon}\right)^{1/2}\left(e^{\frac{qVo}{kT}} - e^{\frac{-qVo}{kT}}\right). \tag{4-24}$$

For $|qV_o/kT| \ll 1$, this gives

$$\sigma \simeq -\frac{\varepsilon}{4\pi}\,\kappa V_o = -\frac{\varepsilon}{4\pi}\,\frac{V_o}{S_2}\,. \tag{4-25}$$

The charge per unit area is larger when the spatial separation is small. This was to be expected, since it is the dipole moment per unit area which gives the electrical potential step to satisfy the condition for no net electron flow between media [Equation (D-5), Appendix D].

Suppose that a film of thickness S_f of liquid oxygen over a hydrogen bubble ruptures. Suppose further that some area A of this film then forms into a droplet of radius r, carrying along the change $q = \sigma A$ from the piece of film. Assuming volume conservation, we have

$$A\,S_f = \frac{4}{3}\,\pi\,r^3. \tag{4-26}$$

The radial electric field at the droplet surface should have a magnitude given by

$$E = \frac{q}{r^2} = (\sigma A)/\left(\frac{3}{4\pi}\,AS_f\right)^{2/3}. \tag{4-27}$$

Using the Approximation (4-25) for σ gives

$$E = -\left(\frac{4\pi}{3}\right)^{2/3}\frac{\varepsilon}{4\pi}\,\frac{A^{1/3}}{S_f^{2/3}}\,\kappa V_o = -\left(\frac{4\pi}{3}\right)^{2/3}\frac{\varepsilon}{4\pi}\,\frac{A^{1/3}}{S_f^{2/3}}\,\frac{V_o}{S_2}. \tag{4-28}$$

Suppose a film area $A = 10^3\,S_f^2$ of oxygen forms a droplet. If $\varepsilon = 1.507$ for oxygen, the space charge layer thickness S_2 is 10^{-5} cm and V_o is 0.05 volt, then the electric field at the droplet surface from Equation (4-28) would be 22,500 volts/cm. Parallel plate breakdown voltage in air at standard conditions is about 31,500 volts/cm and in hydrogen gas is 17,500 volts/cm; this droplet charging to the verge of electric discharge is quite plausible.

We note that at atmospheric pressure oxygen melting temperature, T = 55°K, Equation (4-19) gives a charge-layer thickness

$$S_2 = 48.7\,n_o^{-1/2}\ \text{cm} \tag{4-29}$$

where current carrier density n_o is in cm^{-3}. For a few charge carrier densities this gives

$$\begin{aligned} S_2 &= 4.87 \times 10^{-6}\ \text{cm} \quad \text{for} \quad n_o = 10^{+14}\ cm^{-3} \\ S_2 &= 4.87 \times 10^{-4}\ \text{cm} \quad \text{for} \quad n_o = 10^{+10}\ cm^{-3} \\ S_2 &= 4.87 \times 10^{-3}\ \text{cm} \quad \text{for} \quad n_o = 10^{+8}\ cm^{-3}. \end{aligned} \tag{4-30}$$

For comparison with semiconductors, room temperature (300°K) germanium and silicon have intrinsic (as opposed to impurity) electron carrier density $n_0 = 2.5 \times 10^{13}$ cm^{-3} and 1.4×10^{10} cm^{-3}, respectively.[15]

Following our postulate of doped semiconductor behavior, let us see what impurity carrier density may occur. Impurities of interest may be of the donor, acceptor, trap type.[15] Donor impurities have electrons at energies slightly below the conduction band, and readily supply electrons to the conduction band by ionization to form a positive ion. Acceptor impurities can capture electrons from the valence band to form negative ions, leaving vacancies or "holes" in the valence band as current carriers. Traps can capture or lose electrons also, altering the carrier density.

Kittel[15] shows that a perfectly pure nonconductor has an intrinsic carrier density $n_0^{(i)}$ given by

$$n_0^{(i)} = 2\,(2\pi kT/h^2)^{3/?}\,(m_e m_h)^{3/4} \exp\,[-E_g/(2kT)] \qquad (4\text{-}31)$$

where m_e and m_h are effective masses of conduction electrons and valence band holes, respectively. E_g is the energy gap width, T is absolute temperature, and h is Planck's constant. If the material is doped with donor type impurities only, Kittel shows that the electron carrier density will be approximately

$$n_0^{(d)} = [2\,(2\pi m_e kT/h^2)^{3/2}\,N_d]^{1/2} \exp\,[-E_d/(2kT)] \qquad (4\text{-}32)$$

where N_d is number density of donor impurities and E_d is the minimal energy increment to move the donor's electron to the conduction band.

Since we do not have good information on electron energy levels and band structure in liquid oxygen and liquid hydrogen, we shall only say that plausible values of E_g, E_d, N_d, m_e, and m_h can give values of n_0 in the range used in Examples (4-30).

A charge distribution in a leaky dielectric of relative dielectric constant ε and conductivity σ relaxes with a time constant τ given (in MKS units) by

$$\tau = \frac{\varepsilon \varepsilon_0}{\sigma} \qquad (4\text{-}33)$$

where ε_0 is $\sim 8.85 \times 10^{12}$ coulomb^2 joule^{-1} meter^{-1}. If the value of σ for oxygen is on the order of 10^{-17} (ohm cm)$^{-1}$ or 10^{-19} (ohm meter)$^{-1}$ as reported by Cassutt et al., for pure liquid hydrogen, then the relaxation time in oxygen would be 1.3×10^8 sec. This says that the charge separation would probably proceed only a very short way toward

the equilibrium distribution at the interface, but very little separated charge could coalesce in film rupture. If the impurity level was such as to make $\sigma = 10^{-8}$ (ohm cm)$^{-1}$, then the time constant would be 0.13 seconds, less than typical bubble rise time. For reference, the conductivity of good conductors is $\sim 10^{6}$ (ohm cm)$^{-1}$, that of good insulators is 10^{-14} to 10^{-22} (ohm-cm)$^{-1}$. Solid state semiconductors have conductivities of order 10^{-9} to 10^{2} (ohm cm)$^{-1}$.

The characteristics which go together are

high electrical conductivity,		low electrical conductivity,
thin regions of charge at interfaces,		thick regions of charge at interfaces,
high charge density at interfaces,	or	low charge density at interfaces,
fast charge relaxation,		slow charge relaxation.

It appears that the parameter domain for hydrogen-oxygen froths in large scale violent mixing may be such as to give droplet charging, but we have many gaps in our information. Also, the interface charge distribution does not need to have proceeded very far toward equilibrium to give some droplet charging.

4.3.2 Droplet Discharge Possibilities

In Equation (4-28) and the discussion following it, supported by Examples 4-30, it was shown as plausible that a droplet be charged to near electrical breakdown in film breakage. A much lower level of single droplet charging could produce breakdown from the collective action of all their charges, similar to the natural phenomenon of lightning.

Consider a region of thickness h over the liquid surface carrying n_v droplets per unit volume with charge q_d on each droplet. Then the electric field at the edge of this layer from droplets inside is (in rationalized MKS)

$$E = \frac{n_v q_d h}{2\varepsilon_o} . \qquad (4\text{-}34)$$

Suppose that each droplet is charged so that its surface field is some fraction ϵ of breakdown field E_B:

$$\epsilon E_B = \frac{q_d}{4\pi\varepsilon_o r_d^2} . \qquad (4\text{-}35)$$

Further assume number of droplets per unit volume n_v is such that droplets occupy fraction β of the total volume in the layer:

$$n_v \frac{4}{3} \pi r_d^3 = \beta \quad . \tag{4-36}$$

If we insert Assumptions (4-35) and (4-36) into Equation (4-34), we can solve for the thickness h needed to give electrical breakdown field at the layer edge, namely

$$h = \frac{2}{3} \frac{r_d}{\beta \xi} \quad . \tag{4-37}$$

Hence, if droplet surface field is fraction $\xi = 0.1$ of breakdown and the droplets occupy fraction $\beta = 0.01$ of the space, and droplets are 10^{-2} cm in radius, a layer h = 6.7 cm thick of these suspended droplets would give electric breakdown field at the surface.

It is obvious that an electric field strength approaching this magnitude would contribute to inductive charging of new droplets with opposite sign as they are formed at the liquid surface. While ejection of droplets of opposite charge would tend to reduce the electric field, it also would give a good opportunity for droplet-droplet discharge.

5.0 ALTERNATIVE IGNITION SOURCES

5.1 COSMIC RAY IGNITION MECHANISMS

High energy charged particles leave a path of ionized atoms and recoiling electrons and atoms along their trajectories. The heating and ionization would be conducive to ignition if the energy deposit per unit particle track length were sufficient. Since the energy deposit per unit track length is orders of magnitude smaller than that required for ignition from a discharge, the cosmic ray ignition can be ruled out as highly improbable.

In an experiment on hydrogen ignition, Yates et al.,[16] varied spacing between small electrode pairs to determine minimum ignition energy and quenching distance. They determined that the energy needed in a discharge for ignition decreases as the electrodes are brought closer together until the quenching distance is reached. Further, they found that at electrode spacings that are less than the quenching distance, the minimum ignition energy goes up because of energy and ion losses to electrodes. With this in mind, one suspects that if the energy deposit per unit track length from a charged particle in a combustible mixture exceeds (smallest discharge energy)/(electrode spacing) needed for ignition, the mixture will ignite. The condition for ignition is then

$$\frac{dE}{ds} > \frac{E_{Ig}}{\ell}$$

where E_{Ig} is minimum energy for ignition with electrode separation ℓ, or

$$\frac{dE}{dM} > \frac{E_{Ig}}{\rho \ell}$$

where dE/dM = energy deposit per unit mass per unit area traversed and

ρ = the mass density of the medium traversed.

The minimum ignition energies and corresponding electrode spacings from Yates et al. for a 65% hydrogen, 35% oxygen mixture are shown in Table 5-1.

TABLE 5-1. Minimum Ignition Energy and Corresponding Electrode Spacing for 16°C 65% Hydrogen, 35% Oxygen Mixing at 14.75 psia

Electrode Spacing ℓ (cm)	Ignition Energy E_{Ig} (joules)	Ignition Energy/Length E_{Ig} (joules/cm)	Ignition Energy/(Mass/area) $E_{Ig}/(\rho\ell)$ [joules/(gm/cm^2)2]
1.016	3.5×10^{-3}	3.4×10^{-3}	6.5
0.508	0.75×10^{-3}	1.5×10^{-3}	2.8
0.330	0.7×10^{-3}	2.1×10^{-3}	4.0

We can compare the values of $E_{Ig}/(\rho\ell)$ with the maximum values of dE/dM along tracks of selected charged particles in the hydrogen-oxygen mixture:[17]

$$\frac{dE}{dM} = 2.46 \times 10^{-8} \frac{\text{joule}}{\text{gm/cm}^2} \quad \text{for } ^{238}\text{U ions at 760 MeV}$$

$$\frac{dE}{dM} = 1.072 \times 10^{-10} \frac{\text{joule}}{\text{gm/cm}^2} \quad \text{for } ^{1}\text{H ions at 0.25 MeV}$$

$$\frac{dE}{dM} = 7.764 \times 10^{-9} \frac{\text{joule}}{\text{gm/cm}^2} \quad \text{for } ^{56}\text{Fe ions at 39 MeV.}$$

Thus, we see that for charged particle traverses we have

$$\frac{dE}{dM} << \frac{E_{Ig}}{\rho\ell}$$

and the mixture will not ignite. Therefore, cosmic ray ignition appears improbable, unless the experimental minimal ignition energies for electric discharges reflect some controlling condition not present for cosmic rays.

5.2 CHEMICAL REACTIONS

One major possible source of heat would be the rapid conversion of ortho to para hydrogen which liberates about 339 calories per mole (cal/mole).[18] At cryogenic temperatures the conversion is catalyzed by the presence of a paramagnetic substance such as oxygen.[19] This liberated heat has long been known as a nuisance in liquid hydrogen storage since it causes rapid evaporation. Considering this possibility, a check was made which revealed that propellant hydrogen is normally catalyzed to 95% para to alleviate such evaporation problems. Since the equilibrium composition would be about 99.9% para at 21°K, about 4% of the hydrogen would

convert on contact with the oxygen providing about 13.6 cal/mole (or 57 joules/mole) of hydrogen added. About 13 joules/mole is needed so the mechanism is plausible, but not probable, since large heat losses from evaporation will prevent heat build-up to ignition temperatures.

6.0 CONCLUSIONS AND RECOMMENDATIONS

Partial explanation and substantiation of autoignition (including the Critical Mass Hypothesis) has been possible. Some contributing and alternative processes have been identified as mechanisms of autoignition; electrostatic ignition stands out as the principal mechanism. It is likely that a number of electrostatic processes are involved. Although probability values for various processes were not calculated, order of magnitude estimates were made which indicated reasonable probability on a qualitative basis. Some questions remain unanswered and some additional work is recommended if a better understanding of the process is needed.

6.1 EXPERIMENTAL RESULTS EXPLAINED BY THEORY IN THIS STUDY

The high energy term of the critical mass equation was determined empirically[1] to have the form:

$$m = K_2 E^2,$$

where m = mass mixed, E = dimensionless mixing energy (E = mixing energy/boiling energy) and K_2 = a constant. A mixing theory developed in this study indicated the same form of expression. The low energy term,

$$m = \frac{K_1}{E},$$

a semi-empirical term based in part on the oscillating plug concept,[1] was not derived in this study. Since the low energy term is only important below the boiling energy, it is not considered very important to real autoignition situations because the mixing energy will normally be much higher than the boiling energy. No tests have been conducted below the boiling energy (see Figure 13, Reference 1).

Predictions of streaming potential charging, based on the bobbing plug concept, indicate that sufficient field can be induced to cause ignition. Furthermore, the charging of droplets at the surface accompanied by droplet to droplet discharge is probably a contributing mechanism (although lack of specific data make this somewhat speculative). Some substantiation of this is found in observations of ignition points on or near the surface in some tests.

6.2 EXPERIMENTAL RESULTS NOT EXPLAINED IN THIS STUDY

One area that is greatly lacking in data is fundamental measurements of charge build-up as a function of mixing. The value of constants in the critical mass equation is determined largely from the LN_2/RP-1 mixing

tests which indicated a critical mass of 2300 lb at boiling energy for ignition of LOX/LH_2 and 2800 lb at boiling energy for LOX/RP-1. The similarity between this data and large scale "real" situations is not readily apparent and cannot be readily supported by theory (nor disproved). Empirical support, however, is reasonably good considering that no test has yielded explosions above the established critical mass curve. Thus, the results are plausible but theoretical explanation is not in hand.

Assessment of probabilities associated with various mechanisms was outside the scope of this study. While some mechanisms appear to have reasonably large probability, assessment of others has not been feasible. Most of the mechanisms which showed reasonable probability in LOX/LH_2 are improbable for LOX/RP-1 mainly because of the much larger ignition requirements. Nevertheless, the S-IVB[3] and PYRO 25,000 lb LOX/RP-1 experiments show definite evidence of the reality of some mechanisms. Droplet-droplet charging may be one possible mechanism (see discussion on droplet-droplet discharges in Section 4.3) but this is very speculative.

6.3 RECOMMENDATION FOR FURTHER WORK

If a more complete theoretical understanding is a highly desired goal we would recommend additional theoretical and experimental work. Whether the explanations are now sufficient is a decision best left to those who wish to apply autoignition principles to real applications. If more complete explanation is needed then the work described below would be highly useful.

6.3.1 Experimental Work

More data on mixing energy versus charge build-up is needed. The LN_2/RP-1 experiments should be expanded and additional tests with two cryogenics (perhaps LN_2/LH_2 or LN_2/LOX) should be carried out. The position of the critical mass curve (as opposed to its shape) is inherently dependent on the results of such tests. It is conceivable that the initial mass could be much higher and that external spark sources are always sufficient to cause premature ignition.

Work is also needed to characterize impurities in the propellants and their role in autoignition. In many cases we have noted that electrostatic properties (e.g., zeta potential, resistivity) are very sensitive to the level of impurities in the substances considered. Autoignition could conceivably be greatly enhanced or inhibited by the presence of impurities.

6.3.2 Theoretical Work

Further experimental work could be accompanied by theoretical work to interpret data. In addition to this, expansion of theoretical work carried out in this study would be very useful, in some cases. Specifically,

further work with bubble evaluation models and with prediction of charging effects is recommended. Expansion of these efforts was started in this study but time and funds were very limiting. It is important to note that expansion of these areas would not be very productive unless carried out on a fairly large scale (1 to 2 man years of effort), since some break-throughs, not easily acquired, would be needed.

APPENDIX

BUBBLE POPULATION MODEL

A.1 GENERAL MODEL

A complete description of the bubble population in a liquid is provided by specifying the distribution of bubbles according to their position and size at any time. In order to do this mathematically, let d^3r denote a volume which is small compared to the dimensions of the liquid container, but large enough to contain many bubbles. Then, define a function $n(\underline{r},R,t)$ such that

$$n(\underline{r},R,t)d^3r\,dR = \begin{cases}\text{average number of bubbles with}\\ \text{center located in } d^3r, \text{ and radius}\\ \text{lying in dR about R, at time t.}\end{cases}$$

In order to derive an equation for $n(\underline{r},R,t)$, suppose that $n(\underline{r},R,t)$ is known for some time t, and compute its value at a later time $t + \Delta t$. Clearly,

$$n(\underline{r},R,t+\Delta t)d^3r - n(\underline{r},R,t)d^3r\,dR = \text{net change in n during } \Delta t. \qquad \text{(A-1)}$$

The net change in n is due to several processes, including

1) production of bubbles in $d^3r\,dR$ by nucleate boiling,

2) net flow of bubbles having a radius R in the range dR into d^3r, either by motion of bubbles relative tc the liquid or by motion of the liquid itself,

3) growth of smaller bubbles into dR and growth of bubbles in dR into larger bubbles,

4) breakup of bubbles in dR into two (or more) smaller components, and

5) coalescence of two (or more) smaller bubbles to form one of radius R in the range dR, and coalescence of bubbles of radius R with one (or more) others(s) to form a larger bubble.

An exact description of all of these processes is probably not within reach of existing theory. However, formal expressions may be written for all of them, as will be done here:

1) Let $s(\underline{r},t)d^3r$ denote the rate that bubbles are produced in d^3r at time t. Let f(R)dR denote the probability that a given bubble is produced by nucleation with radius R in the range dR. Since f(R) is a probability distribution, it is normalized so that

$$\int_0^\infty f(R)dR = 1.$$

In terms of s and f, the number of bubbles produced in $d^3r\ dR$ during a (small) time Δt is $s(\underline{r},t)f(R)d^3r\ dR\ \Delta t$.

2) Let $\underline{j}(\underline{r},R,t)$ denote the current of bubbles. Then, by familiar arguments, the net flow of bubbles of radius R in the range dR into d^3r during time Δt is given by $-\nabla\cdot\underline{j}(\underline{r},R,t)d^3r\ dR\ \Delta t$.

3) Let $G(R \to R',\Delta t)dR'$ denote the probability that a bubble of radius R will grow to a radius R' in the range dR' during Δt. Then the number of bubbles in d^3r with radius R in the range dR, which grow to a new radius R' in the range dR' during Δt, is given by $n(\underline{r},R,t)d^3r\ dR \cdot G(R \to R',\Delta t)dR'$. Thus, the total number of bubbles leaving dR by this mechanism during time Δt is given by

$$n(r,R,t)d^3r\ dR \cdot \int_R^\infty G(R \to R',\ \Delta t)dR'.$$

By a similar argument, the total number of bubbles entering dR, due to growth from $R' < R$, is given by

$$\int_0^R n(\underline{r},R',t)G(R' \to R,\ \Delta t)dR' \cdot d^3r\ dR.$$

To proceed further with these expressions, a model is needed to describe $G(R' \to R,\Delta t)$. The simplest model is a deterministic growth model which is based on the assumption that the growth rate of the bubble radius depends only on its present radius, i.e.,

$$\frac{dR}{dT} = G(R)$$

for some function G(R). For this model, $R(t + \Delta t)$ must have the value $R(t) + G[R(t)] \cdot \Delta t$, i.e., $G(R \to R',\Delta t) = \delta[R' - R - G(R)\Delta t]$. With this expression for $G(R \to R',\Delta t)$, the above integrals are easily evaluated to give

$$\text{growth out of } dR = n(\underline{r},R,t)d^3r\ dR, \text{ and}$$
$$\text{growth into } dR = n(\underline{r},R - G(R)\Delta t,t)d^3r\ dR.$$

Therefore, since Δt is small

$$\text{growth into } dR \simeq \left[n(\underline{r},R,t) - G(R)\ \frac{\partial n}{\partial R}\ (\underline{r},R,T)\Delta t\right] d^3r\ dR.$$

4) In the expression for bubble breakup, we include only the spontaneous breakup rate which is a function of R alone. (At higher bubble

densities, stimulated breakup, which is caused by the passage of one or more bubbles near another, may also contribute, but this process will not be considered here.) We let $B(R \rightarrow R',R")dR'dr"$ denote the rate at which bubbles of radius R break up to form a pair of bubbles with radii R' in the range dR' and R" in the range dR". Then, the number of bubbles leaving $d^3r\ dR$ during Δt, due to breakup, is given by $n(\underline{r},R,t)d^3r\ dR \cdot B(R) \cdot \Delta t$, where

$$B(R) = \int_0^R \int_0^R B(R \rightarrow R',R")dR'dR".$$

Similarly, the number of bubbles entering dR during Δt, due to breakup of larger bubbles, is given by

$$\int_R^\infty n(\underline{r},R',t)B(R' \rightarrow R)dR' \cdot d^3r \cdot \Delta t$$

where $B(R' \rightarrow R) = \int_R^\infty B(R' \rightarrow R,R")dR" + \int_R^\infty B(R' \rightarrow R",R)dR".$

5) Coalescence is basically the inverse of breakup. Here, two bubbles of radii R' and R" merge to form a new bubble of radius R. (At higher bubble densities, interactions between three and more bubbles may also contribute, but this process will not be considered here.) Let $C(R',R" \rightarrow R)dR$ denote the rate at which bubbles of radii R' and R", both located in d^3r, coalesce to form a new bubble of radius R in the range dR. Then, the number of bubbles leaving dR during Δt, due to coalescence, is given by

$$n(\underline{r},R,t)d^3r\ dR \cdot \int_0^\infty n(\underline{r},R',t)C(R,R')dR'\ \Delta t$$

where

$$C(R,R') = \int_R^\infty C(R,R' \rightarrow R")dR".$$

Similarly, the number of bubbles added to dR, due to coalescence of two smaller bubbles during Δt, is

$$\int_0^R \int_0^R n(\underline{r},R',t)n(\underline{r},R",t)C(R',R" \rightarrow R)dR'dR" \cdot dR \cdot \Delta t.$$

At this point, formal expressions have been given for each process that contributes to the right hand side of Equation (A-1). When these

expressions are substituted, each term in the resulting equation contains the factors $d^3r\ dR$ which can be cancelled. Then, if the equation is divided by Δt and the limit $\Delta t \to 0$ is taken. the result is

$$\frac{\partial n}{\partial t} + G(R)\frac{\partial n}{\partial R} + B(R)n = -\nabla \cdot \underline{j} + s(\underline{r},t)f(R) + \int_R^\infty n(R')B(R' \to R)dr'$$

$$+ \int_0^R \int_0^R n(R')n(R'')C(R',R'' \to R)dR'dR''$$

$$- n(R)\int_0^\infty n(R')C(R,R')dR'. \qquad \text{(A-2)}$$

This equation is not yet tractable, since it is necessary to specify the current $\underline{j}$ separately, and to provide models for $G(R)$, $B(R' \to R)$, $C(R',R'' \to R)$ and $f(R)$. Thus, some simplifications to this general equation, which lead to more tractable forms, will be discussed in the following subsection.

A.2 SIMPLIFICATIONS TO THE GENERAL MODEL

At low bubble densities the coalescence terms will be negligible compared to other terms, which lead to

$$\frac{\partial n}{\partial t} + G(R)\frac{\partial n}{\partial R} + B(R)n = -\nabla \cdot \underline{j} + s(\underline{r},t)f(R) + \int_R^\infty n(R')B(R' \to R)dr'.$$

If, in addition, no very large bubbles are present in the system, the spontaneous breakup terms will be small, which lead to

$$\frac{\partial n}{\partial t} + G(R)\frac{\partial n}{\partial R} = -\nabla \cdot \underline{j} + s(\underline{r},t)f(R).$$

If the bubble velocity depends only on size, the current $\underline{j}$ can be written as

$$\underline{j}(\underline{r},R,t) = \underline{v}(R)n(\underline{r},R,t).$$

In this case, the equation for n reduces to

$$\frac{\partial n}{\partial t} + G(R)\frac{\partial n}{\partial R} + \underline{v}(R) \cdot \nabla n = s(\underline{r},t)f(R). \qquad \text{(A-3)}$$

In this form the equation is tractable if models are available to specify $G(R)$, $\underline{v}(R)$ and $f(R)$. In fact, since

$$G(R) = \frac{dR}{dt} \text{ and } \underline{v}(R) = \frac{d\underline{r}}{dt}$$

for a bubble of radius R and position $\underline{r}$, Equation (A-3) simply states that

$$\frac{dn}{dt} = s(\underline{r},t)f(R). \qquad \text{(A-4)}$$

Here, $\frac{d}{dt}$ denotes the total time derivative along the characteristic curves, $R = R(t)$ and $\underline{r} = \underline{r}(t)$, which are determined by integrating

$$\frac{dR(t)}{dt} = G[R(t)] \qquad \text{(A-5a)}$$

$$\frac{d\underline{r}(t)}{dt} = \underline{v}[R(t)]. \qquad \text{(A-5b)}$$

The solution of Equations (A-4), (A-5a) and (A-5b) for a particular case is given in Section A.3.

A.3 SOLUTION FOR TWO ADJACENT FLUIDS - GENERAL

Suppose that two fluids of different temperature are brought together at time $t = 0$. Idealize the geometry so that Fluid 1 occupies part of the upper half-space $0 < Z < h$, while Fluid 2 occupies part of the lower half-space $-b < Z < 0$. Suppose the temperature of Fluid 1 is less than that of Fluid 2 and that both fluids are initially saturated liquids. A thermal boundary layer will form in both fluids with nucleate boiling occurring in the boundary layer of Fluid 1 and (possibly) ice crystals forming in the boundary layer of Fluid 2. Due to buoyancy, vapor bubbles of Fluid 1 will rise out of the boundary layer as saturated vapor and into the bulk of Fluid 1. If Solid 2 has greater density than Liquid 2, any ice crystals formed in the boundary layer of Fluid 2 will sink into the bulk of Fluid 2 as saturated ice (Figure A-1).

The description of the bubble population requires consideration of two regimes: 1) bubble nucleation and growth in the boundary layer, and 2) bubble rising and growth above the boundary layer. These two regimes require separate analyses which are outlined below.

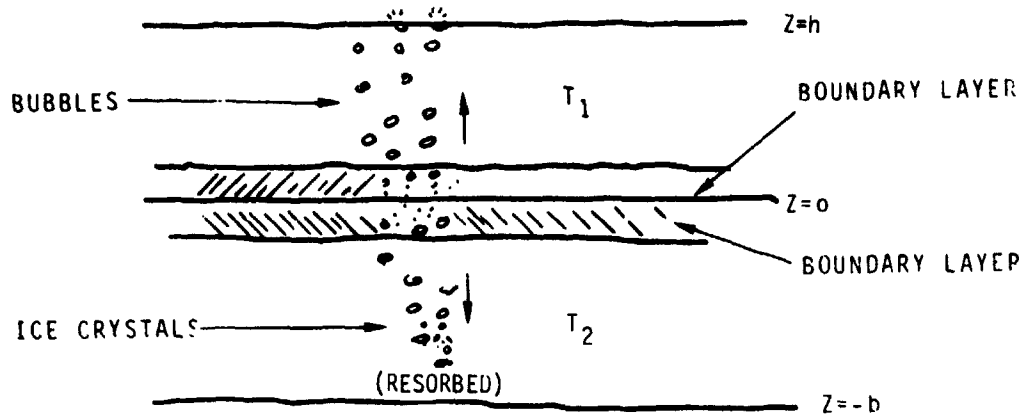

FIGURE A-1. A Two-Fluid Model

A.3.1 The Boundary Layer

In the thermal boundary layer, which forms when the two fluids at their boiling points come into contact, the colder fluid will be superheated. The formation and growth of bubbles in a superheated region have been studied in some detail[20] with the conclusion that the radius of a growing bubble expands as

$$R(t) = \bar{K}t^{1/2} \tag{A-6}$$

where $\bar{K}$ is a constant depending on fluid prcperties and the degree of superheating. With the expression for R(t) known explicitly, some of the factors appearing on the equation for n (r,R,t) can be determined. In particular, from Equation (A-6)

$$\frac{dR}{dt} = \frac{\bar{K}}{2} t^{-1/2} = \frac{\bar{K}^2}{2R} . \tag{A-7}$$

Thus, from Equation (A-5a), we have

$$G(R) = \frac{\bar{K}^2}{2R} . \tag{A-8}$$

The velocity v(R) can also be determined if we assume that the bubble velocity is vertical and is due to the combined effect of buoyancy and gravity forces. Then,

$$\underbrace{\frac{4}{3}\pi R^3 \cdot \rho_b \frac{dv}{dt}}_{\text{net force}} = \underbrace{\frac{4}{3}\pi R^3 \rho g}_{\text{buoyancy}} - \underbrace{6\pi\mu R v}_{\text{drag}} \qquad \text{(A-9)}$$

where

ρ_b = bubble density

ρ = fluid density, and

μ = viscosity.

Thus,

$$\frac{dv}{dt} + \frac{9\mu}{2\rho_b R^2} v = \frac{\rho g}{\rho_b} . \qquad \text{(A-10)}$$

Dividing Equation (A-10) by Equation (A-7) gives

$$\frac{dv}{dR} + \frac{C_1}{R} v = C_2 R \qquad \text{(A-11)}$$

where

$$C_1 = \frac{9\mu}{\bar{K}^2 \rho_b} \text{ and } C_2 = \frac{2\rho g}{\bar{K}^2 \rho_b} .$$

Here, we take ρ_b = constant throughout the boundary layer since the boundary layer is thin. The solution of Equation (A-11) is then

$$v(R) = \left(\frac{C_2}{C_1 + 2}\right) R^2 \qquad \text{(A-12)}$$

which provides v(R) (assumed in +Z direction) for Equation (A-4). From Equations (A-5b), (A-12) and (A-6) we also obtain

$$\frac{dZ}{dt} = \left(\frac{C_2 \bar{K}^2}{C_1 + 2}\right) t \qquad \text{(A-13)}$$

where Z is the vertical component of r. Thus,

$$Z(t) = Z_0 + \frac{C_2\bar{K}^2}{2(C_1 + 2)}\, t^2 \qquad \text{(A-14)}$$

where Z_0 is the height at which the bubble first forms by nucleation.

As an illustration of how Equation (A-4) can be solved for n(Z,R,t), we consider the case where one bubble nucleates at Z = 0 at time t = 0. Then, according to Equation (A-4)

$$\frac{dn}{dt} = 0 \text{ for } Z > 0,\ t > 0.$$

Thus, n is constant along the curves given by solving Equations (A-5a) and (A-5b). Since these have already been solved [Equations (A-6) and (A-14) above] for the present simple model, we have for one bubble

$$n(Z,R,t) = \delta\left[Z - \frac{C_2\bar{K}^2}{2(C_1 + 2)}\, t^2\right] \delta\left(R - \bar{K}t^{1/2}\right) \qquad \text{(A-15)}$$

where δ = a dirac delta function.

If, instead of one bubble, we consider the continuous production of bubbles at Z = 0, starting at time t = 0 at a rate of S bubbles per cm^3 sec, then we integrate Equation (A-15) from 0 to t to obtain

$$n(Z,R,t) = \frac{S}{\sqrt{AZ}}\, \delta\left[R - \bar{K}\left(\frac{Z}{A}\right)^{1/4}\right] H\left[t - \left(\frac{Z}{A}\right)^{1/2}\right] \qquad \text{(A-16)}$$

where

$$A = \frac{C_2\bar{K}^2}{2(C_1 + 2)}$$

and H denotes the step function

$$H(t) = \begin{cases} 1 & t > 0 \\ 0 & t < 0 \end{cases}$$

Equation (A-16) shows that at a given position Z all bubbles have the same radius and that bubbles arrive at height Z only after a time $(Z/A)^{1/2}$. In particular, if h is the height of the thermal boundary layer then

$$n(h,R,t) = \frac{S}{\sqrt{Ah}}\,\delta\left(R - \overline{K}\left(\frac{h}{A}\right)^{1/4}\right) H\left(t - \left(\frac{h}{A}\right)^{1/2}\right). \qquad \text{(A-17)}$$

This expression must now be used as a boundary condition for analyzing the bubble population in the second regime, i.e., above the boundary layer.

A.3.2 The Bulk Fluid Above the Boundary Layer

In the region above the boundary layer, the assumptions of the model are somewhat different. Here, the bubble no longer grows by evaporating more superheated liquid (since there is none), but rather by responding to changes in pressure and temperature as it rises. Since the pressure is likely to vary as the bubble rises, it is no longer adequate to treat the bubble density ρ_b as a constant, nor can it be assumed that the bubble contains pure saturated vapor. In order to describe the bubble dynamics in this regime, a number of basic equations are needed. These are derived below.

The Mass Equation

For a fluid in general, we have

$$\frac{\partial \rho}{\partial t} + \nabla \cdot \rho \underline{v} = 0. \qquad \text{(A-18)}$$

Integrate this equation over the bubble volume V(t), with surface S(t), to get

$$\int_{V(t)} \frac{\partial}{\partial t}\,\rho\, d^3r + \int_{V(t)} \nabla \cdot \rho \underline{v}\, d^3r = 0. \qquad \text{(A-19)}$$

Use Leibnitz's and Gauss' theorems to transform

$$\left(\frac{d}{dt}\int_{V(t)} \rho d^3r - \int_{S(t)} \rho \underline{v}_s \cdot \underline{n}_s\, d^2S\right) + \int_{S(t)} \rho \underline{v} \cdot \underline{n}_s\, d^2S = 0. \qquad \text{(A-20)}$$

Here, S(t) = surface, $\underline{n}_s$ = outer normal to surface, d^2S = element of area on S(t), $\underline{v}_s$ = velocity of surface point.

Let

$$M(t) = \int_{V(t)} \rho d^3r = \text{bubble mass}. \qquad \text{(A-21)}$$

Then,

$$\frac{dM}{dt} = \int_{S(t)} \rho(\underline{v}_S - \underline{v}) \cdot \underline{n}_S \, d^2S = \text{evaporation rate.} \qquad \text{(A-22)}$$

The Energy Equation

For a fluid in general

$$\frac{\partial}{\partial t} \cdot \rho \left(u + \frac{v^2}{2} + gZ\right) + \nabla \cdot \rho\underline{v}\left(h + \frac{v^2}{2} + gZ\right) = \nabla \cdot (\underline{\underline{\tau}} \cdot \underline{v} - \underline{J}) + \rho g v_Z. \qquad \text{(A-23)}$$

(Here, +Z = upward) Integrate this equation over V(t), then use Leibnitz's and Gauss' theorems to get

$$\frac{d}{dt}\int_{V(t)} \rho\left(u + \frac{v^2}{2} + gZ\right) d^3r - \int_{S(t)} \rho \left(u + \frac{v^2}{2} + gZ\right) \underline{v}_S \cdot \underline{n}_S \, d^2S$$

$$+ \int_{S(t)} \rho \left(h + \frac{v^2}{2} + gZ\right) \underline{v} \cdot \underline{n}_S \, d^2S = \int_{S(t)} (\underline{\underline{\tau}} \cdot \underline{v} - \underline{J}) \cdot \underline{n}_S \, d^2S$$

$$+ g \int_{V(t)} \rho v_Z \, d^3r. \qquad \text{(A-24)}$$

Expect that kinetic energy terms ($\frac{v^2}{2}$) are small and that dissipation heat ($\int_S \underline{\underline{\tau}} \cdot \underline{v} \cdot \underline{n}_S \, d^2S$) is negligible. Then, since $h = u + P/\rho$,

$$\frac{d}{dt}\int_{V(t)} \rho u d^3r = \int_{S(t)} \rho(u + gZ)(\underline{v}_s - v) \cdot \underline{n}_s \, d^2S - \int_{S(t)} P\underline{v} \cdot \underline{n}_s \, d^2S$$

$$- g \frac{d}{dt}\int_{V(t)} \rho Z \, d^3r + g\int_{V(t)} \rho v_Z \, d^3r - \int_{S(t)} \underline{J} \cdot \underline{n}_s \, d^2S. \qquad \text{(A-25)}$$

Also, the potential energy terms cancel since

$$PE = \int_V \rho g Z \, d^3r.$$

Therefore,

$$\frac{d(PE)}{dt} = g \frac{d}{dt}\int_V \rho Z \, d^3r = g\left(\int_V Z \frac{\partial \rho}{\partial t} \, d^3r + \int_s \rho Z \underline{v}_s \cdot \underline{n}_s \, d^2S\right)$$

$$= g\left(-\int_V Z\nabla \cdot \rho\underline{v} \, d^3r + \int_s \rho Z \underline{v}_s \cdot \underline{n}_s \, d^2S\right)$$

$$= g\left(-\int_V \nabla \cdot \rho\underline{v}Z \, d^3r + \int_V \rho\underline{v} \cdot \nabla Z \, d^3r + \int_s \rho Z \underline{v}_s \cdot \underline{n}_s \, d^2S\right)$$

$$= g\left(-\int_s \rho\underline{v}Z \cdot \underline{n}_s \, d^2S + \int_V \rho v_Z \, d^3r + \int_s \rho v_s Z \cdot \underline{n}_s \, d^2S\right)$$

$$= g\left(\int_V \rho v_Z \, d^3r + \int_s \rho Z \, (\underline{v}_s - \underline{v}) \cdot \underline{n}_s \, d^2S\right)$$

and

$$g \frac{d}{dt}\int_V \rho Z \, d^3r = g\int_V \rho v_Z \, d^3r + g\int_s \rho Z \, (\underline{v}_s - \underline{v}) \cdot \underline{n}_s \, d^2S. \qquad \text{(A-26)}$$

Thus, the energy equation becomes

$$\frac{d}{dt}\int_{V(t)} \rho u \, d^3r = \int_{S(t)} \rho u \, (\underline{v}_s - \underline{v}) \cdot \underline{n}_s \, d^2S - \int_{S(t)} P\underline{v} \cdot \underline{n}_s \, d^2S$$

$$- \int_{S(t)} \underline{J} \cdot \underline{n}_s \, d^2S. \qquad \text{(A-27)}$$

Take u and P uniform across V; let J denote last integral; then

$$\frac{d}{dt}(Mu) = u\int_s \rho \, (\underline{v}_s - \underline{v}) \cdot \underline{n}_s \, d^2S - P\int_s \underline{v} \cdot \underline{n}_s \, d^2S - J.$$

Since the first integral is $\frac{dM}{dt}$ from the mass equation,

$$M\frac{du}{dt} = - P\int_s \underline{v} \cdot \underline{n}_s \, d^2S - J.$$

Under integral sign, take $\pm v_s$ to get

$$-\int_s \underline{v} \cdot \underline{n}_s \, d^2S = \int_s (v_s - v) \cdot \underline{n}_s \, d^2S - \int_s \underline{v}_s \cdot \underline{n}_s \, d^2S$$

Since

$$V = \int_{V(t)} d^3r, \quad \frac{dV}{dt} = \int_s \underline{v}_s \cdot \underline{n}_s \, d^2S$$

that is

$$-\int_s \underline{v} \cdot \underline{n}_s \, d^2S = \int_s (\underline{v}_s - \underline{v}) \cdot \underline{n}_s \, d^2S - \frac{dV}{dt}$$

then the energy equation becomes

$$M \frac{du}{dt} = P \int_S (\underline{v}_s - \underline{v}) - \underline{n}_s \, d^2S - P \frac{dV}{dt} - J \qquad \text{(A-28)}$$

The Momentum Equation

For a fluid in general

$$\frac{\partial}{\partial t} \rho \underline{v} + \nabla \cdot \rho \underline{v}\underline{v} = - \nabla P + \nabla \cdot \underline{\underline{\tau}} - \rho g \hat{z} \, . \qquad (\hat{z} = \text{unit vector up}) \qquad \text{(A-29)}$$

Integrate over V(t) and convert integrals to get

$$\frac{d}{dt} \int_V \rho \underline{v} \, d^3r - \int_S \rho \, \underline{v} \, \underline{v}_s \cdot \underline{n}_s \, d^2S + \int_S \rho \, \underline{v} \, \underline{v} \cdot \underline{n}_s \, d^2S$$

$$= - \int_S P \, \underline{n}_s \, d^2S + \int_S \underline{\underline{\tau}} \cdot \underline{n}_s \, d^2S - g\hat{z} \int_V \rho \, d^3r$$

i.e.,

$$\frac{d}{dt} \int_V \rho \, \underline{v} \, d^3r = \int_S \rho \underline{v} \, (\underline{v}_s - \underline{v}) \cdot \underline{n}_s \, d^2S - \int_S P \, \underline{n}_s \, d^2S$$

$$+ \int_S \underline{\underline{\tau}} \cdot \underline{n}_s \, d^2S - g\hat{z}M.$$

Note that

$$\int_S P \, \underline{n}_s \, d^2S = \text{buoyant force} = - \frac{\rho_L}{\rho} M \, g\hat{z}$$

where ρ_L is the liquid density and ρ the bubble density. Also,

$$\int_S \underline{\underline{\tau}} \cdot \underline{n}_S \, d^2S = \text{drag force} \simeq - 6\pi\mu R\underline{v}_B$$

$$= - 6\pi\mu \left(\frac{3M}{4\pi\rho}\right)^{1/3} \underline{v}_B$$

(Here, $\underline{v}_B$ refers to the mean bubble velocity.)

i.e.,

$$\frac{d}{dt} \int_V \rho\underline{v} \, d^3r = \int_S \rho\underline{v} \, (\underline{v}_S - \underline{v}) \cdot \underline{n}_S \, d^2S + \frac{\rho_L}{\rho} \, Mg\hat{z}$$

$$- 6\pi\mu R\underline{v}_B - gM\hat{z}. \qquad \text{(A-30)}$$

In the first integral, approximate $\underline{v}$ by $\underline{v}_B$ to get $\int_V \rho\underline{v} \, d^3r \simeq M\underline{v}_B$. In the second integral, replace the first $\underline{v}$ factor by $\underline{v}_B$. This is allowed if flow velocity into surface (due to condensation or evaporation) is small compared to mean bubble velocity. Then,

$$\frac{d}{dt} M\underline{v}_B = \underline{v}_B \int_S \rho \, (\underline{v}_S - \underline{v}) \cdot \underline{n}_S \, d^2S + \frac{\rho_L}{\rho} \, Mg\hat{z} - 6\pi\mu R\underline{v}_B - gM\hat{z}.$$

The integral is $\frac{dM}{dt}$ from the mass equation so

$$M \frac{d\underline{v}_B}{dt} = - 6\pi\mu R\underline{v}_B + \left(\frac{\rho_L}{\rho} - 1\right) Mg\hat{z}. \qquad \text{(A-31)}$$

Second Law of Thermodynamics

In a system where M changes and heat dQ is transferred in, we have

$$dS \geq \frac{dQ}{T} + s dM, \quad \text{i.e., } dQ \leq TdS - TsdM. \tag{A-32}$$

Thus, for the bubble

$$-J \equiv \frac{dQ}{dt} \leq T\frac{ds}{dt} - Ts\frac{dM}{dt}$$

or with $S = sM$,

$$-J \leq T\frac{ds}{dt} - s\frac{dM}{dt}$$

or

$$-J \leq TM\frac{ds}{dt}.$$

For reversible case, note $J = 0$ implies that s = constant.

Pressure Discontinuity at Surface

$$P\ (\text{bubble}) = P\ (\text{liquid}) + \frac{2\sigma}{R} \qquad (\sigma = \text{surface tension}) \tag{A-34}$$

Ideal Vapor Inside Bubble

If specific heat is constant and $s = 0$ at $T = T_1$, $P = P_1$ then

$$P = \rho_v rT$$

$$s_v(P,T) = C_{pv}\ln\ (T/T_1) - r\ \ln\ (P/P_1) \tag{A-35}$$

$$u_v(P,T) = (C_{pv} - r)\ (T - T_1). \tag{A-36}$$

This analysis also applies when there are small liquid droplets within the bubble.

Hydrostatic Pressure

$$P \text{ (liquid)} = P_0 - \rho_L g z \qquad \text{(A-37)}$$

where z = distance above point where $P = P_0$.

Geometry

$$V = \frac{4}{3}\pi R^3. \qquad \text{(A-38)}$$

Density

$$M = \rho V. \qquad \text{(A-39)}$$

Displacement

This is same as for boundary layer regime, i.e.,

$$\frac{dz}{dt} = v_z. \qquad \text{(A-40)}$$

A.4 SIMPLIFIED BULK FLUID MODEL

Look at the simplest case: no mass or heat transfer ($\frac{dM}{dt} = 0$, $J = 0$). This does not rule out condensation of tiny droplets inside the bubble. It just means that they stay in the bubble as mist rather than being absorbed into the surrounding liquid.

We now have from mass equation [Equation (A-22)]:

$$\frac{dM}{dt} = 0 \tag{A-41}$$

with solution

$$M(t) = M_0. \tag{A-42}$$

From second law ([Equation (A-33)] have $\frac{ds}{dt} \geq 0$. Approximate by reversible case $\frac{ds}{dt} = 0$, i.e.,

$$s(t) = s(0). \tag{A-43}$$

Now, we can estimate the state of the bubble, which presumably leaves the boundary layer as saturated pure vapor. In rising into a lower pressure region at constant s, we must determine whether it superheats or, instead, changes to a mixture of saturated vapor plus droplets. In the former, pure vapor, case Equation (A-37) predicts that

$$\frac{P}{P_0} = \left(\frac{T}{T_0}\right)^{C_{P/r}} = 1-\left(1-\frac{T}{T_0}\right)^{C_{P/r}}$$

$$\simeq 1- \frac{C_p}{r}\left(1- \frac{T}{T_0}\right) \quad \text{for } T \text{ near } T_0. \tag{A-44}$$

If, instead, a vapor-liquid mixture results, then P is given by the saturation pressure $P_S(T)$. From corresponding state theory, $\frac{P}{P_c}$ should be a universal function of $\frac{T}{T_c}$ (c = critical point). In practice, this is approximate, and is given by the empirical fit[21]

$$P_s(T) \simeq P_c \exp\left[5.29 - 5.31\left(\frac{T_c}{T}\right)\right]. \tag{A-45}$$

Thus,

$$\frac{P_s(T)}{P_0} \simeq e^{-5.31\ T_c\left(\frac{1}{T} - \frac{1}{T_0}\right)} \equiv f(T)$$

where

$$(T_0,\ P_0 \text{ at } t = 0).$$

Then

$$f'(T) = \frac{5.31\ T_c}{T^2} \times f(T)$$

and

$$f(T) \simeq f(T_0) + (T-T_0)\ f'(T_0) + \ldots$$

$$\frac{P_s(T)}{P_0} \simeq 1 - 5.31\left(\frac{T_c}{T_0}\right)\left(1 - \frac{T}{T_0}\right) \quad \text{for } T \text{ near } T_0. \qquad \text{(A-46)}$$

Thus, the coefficient of $\left(1 - \frac{T}{T_0}\right)$ is $5.31\left(\frac{T_c}{T_0}\right)$ for the liquid-vapor mixture and $C_{\rho/r} \approx 3/2$ for the pure vapor (see Figure A-2). Cooling at constant s leads immediately into the liquid region, so the liquid-vapor case is the one that occurs.

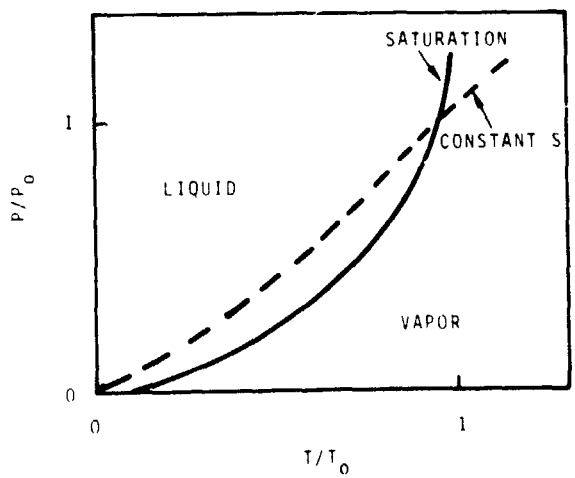

FIGURE A-2. Sketch of Pressure Temperature Data

Since hydrostatic pressure is assumed, we have [Equation (A-37)]

$$P_L = P_0 - \rho_L\, gZ.$$

Neglect surface tension so that

$$P(Z) = P_0 - \rho_L\, gZ.$$

Since the bubble is at saturation pressure, we have

$$P_s(T) = P_0 - \rho_L\, gZ$$

which determines $T(Z)$, i.e.,

$$T(Z) = T_{sat}\,(P_0 - \rho_L\, gZ).$$

If the corresponding states expression is used, this gives

$$T(Z) = \frac{5.31\, T_c}{5.29 - \ln\left(\dfrac{P_0 - \rho_L\, gZ}{P_c}\right)}$$

or with $T = T_0$ at $z = 0$,

$$T(Z) \simeq T_0 \left[\frac{5.29 + \ln\left(P_c/P_0\right)}{5.29 + \ln\left(\dfrac{P_c}{P_0 - \rho_L\, gZ}\right)}\right]. \qquad \text{(A-47)}$$

Note that as i increases, T decreases.

To continue, the assumption of ideal vapor gives

$$\rho_v = P/rT$$

or

$$\rho_v\,(Z) = P(Z)/rT(Z).$$

Also,

$$s_v\,(Z) = C_{pv} \ln\left(\frac{T(Z)}{T_1}\right) - r \ln\left(\frac{P(Z)}{P_1}\right) \qquad \text{(A-48)}$$

For the liquid, assume incompressibility so that

$$\rho_L\,(Z) = \rho_L = \text{const}$$

$$s_L\,(Z) = C_{pL} \ln\,(T/T_2)$$

where T_2 is a reference temperature.

With the above models we can construct the remaining properties: Since

$$M_L + M_v = M$$

and

$$\frac{M_L}{\rho_L} + \frac{M_v}{\rho_v} = V$$

we have, after a little algebra,

$$\frac{M_v}{M} = \rho_v \left(\frac{1}{\rho} - \frac{1}{\rho_L}\right) \Big/ \left(1 - \frac{\rho_v}{\rho_L}\right) \qquad \text{(A-49)}$$

and

$$\frac{M_L}{M} = \left(1 - \frac{\rho_v}{\rho}\right) \Big/ \left(1 - \frac{\rho_v}{\rho_L}\right) \qquad \text{(A-50)}$$

Thus,

$$s = \frac{M_v}{M} s_v + \frac{M_L}{M} s_L$$

$$= \frac{1}{\left(1 - \frac{\rho_v}{\rho}\right)} \left\{ \rho_v \left(\frac{1}{\rho} - \frac{1}{\rho_L}\right) \left[C_{pv} \ln\left(T/T_1\right) - r \ln\left(P/P_1\right) \right] \right.$$

$$\left. + \left(1 - \frac{\rho_v}{\rho}\right) \left[C_{pL} \ln\left(1/T_2\right) \right] \right\}. \qquad \text{(A-51)}$$

Now, since s is to be constant = $s_0 = C_{pv} \ln\left(\frac{T_0}{T_1}\right) - r \ln\left(\frac{P_0}{P_1}\right)$ (since the bubble is initially pure vapor), we must have

$$\frac{1}{1 - \frac{\rho_v}{\rho}} \left\{ \rho_v \left(\frac{1}{\rho} - \frac{1}{\rho_L}\right) \left[C_{pv} \ln\left(T/T_1\right) - r \ln\left(P/P_1\right) \right] \right.$$

$$\left. + \left(1 - \frac{\rho_v}{\rho}\right) C_{pL} \ln\left(1/T_2\right) \right\} = C_{pv} \ln\left(\frac{T_0}{T_1}\right) - r \ln\left(\frac{P_0}{P_1}\right)$$

which can be solved for ρ to get

$$\rho(Z) = \frac{\rho_v(Z)\, Q(Z)}{T(Z) \left(1 - \frac{\rho_v(Z)}{\rho_L(Z)}\right) \left[C_{pv} \ln\left(\frac{T_0}{T_1}\right) - r \ln\left(\frac{P_0}{P_1}\right) - C_{pL} \ln\left(\frac{T(Z)}{T_2}\right) \right]} \qquad \text{(A-52)}$$

in which

$$s_v - s_L = Q/T$$

with Q the latent heat of vaporization $\left[Q(Z) \equiv Q\,[T(Z)]\right]$.

Then

$$R(Z) = \left[\frac{3}{4\pi}\left(\frac{M_o}{\rho(Z)}\right)\right]^{1/3} = \left[\frac{\rho_o}{\rho(Z)}\right]^{1/3} R_o \qquad \text{(A-53)}$$

where ρ_o, R_o = ρ,R at boundary layer interface. It remains to find the velocity v(Z) and the position Z(T). We note at this stage that u(Z) can be determined just as s(Z) was by taking $u = \frac{M_v}{M} u_v + \frac{M_L}{M} u_L$. Thus, the energy equation should give no new information as can be seen if we rewrite Equation (A-28) using $V = \frac{M_0}{\rho}$ and $\frac{d}{dt} = v \frac{d}{dZ}$ to get

$$M_0 \, v \, \frac{du}{dZ} = \frac{PM_0}{\rho^2} \, v \, \frac{d\rho}{dZ} \qquad \text{(A-54)}$$

i.e.,

$$\frac{du}{dZ} - \frac{P}{\rho^2} \frac{d\rho}{dZ} = 0 \qquad \text{(A-55)}$$

which is satisfied identically since $\frac{dh}{dZ} - \frac{1}{\rho} \frac{dP}{dZ} = T \frac{ds}{dZ} = 0$.

To solve for v, rewrite Equation (A-31) using $V = M_0/\rho$ and

$$\frac{d}{dt} = v \frac{d}{dZ}$$

to get

$$v \frac{dv}{dZ} = - \frac{6\pi\mu R}{M_0} v + \left(\frac{\rho_L}{\rho} - 1\right) g . \qquad \text{(A-56)}$$

Since R(Z) and ρ(Z) are known, Equation (A-56) is of the form

$$v \frac{dv}{dZ} + f(Z) \, v = h(Z)$$

with f and h known. This is apparently not solvable in closed form,[22] even for simple f and h, although it can be solved numerically. For numerics, write as

$$\frac{dv}{dZ} = \frac{h(Z)}{v} - f(Z)$$

so that

$$v(Z) = \left(v_0 - \int_0^Z f(Z')dZ'\right) + \int_0^Z \frac{h(Z')}{v(Z')}\,dZ'$$

which is a nonlinear integral equation for v(Z). It can probably be solved successfully by iteration.

Once v(Z) is determined, the position Z(t) follows from Equation (A-40):

$$\frac{dZ}{dt} = v(Z)$$

or

$$\frac{dZ}{v(Z)} = dt$$

or

$$\int_0^Z \frac{dZ'}{v(Z')} = t.$$

With Z(t) determined, all other quantities available as functions of Z become explicit functions of t.

It is disappointing that even this simplest case seems to require one numerical solution [v(Z)]; but perhaps it is surprising that all but one equation <u>can</u> be integrated in closed form.

With all quantities related to an individual bubble as determined above, the distribution function n(Z,R,t) can also be determined. Assuming that no bubbles form by nucleation above the boundary layer, and that the distribution of bubbles entering from the boundary layer at Z = h is given by Equation (A-17).

APPENDIX B

DETAILED DEVELOPMENT OF MIXING MODEL

This model is concerned with the high energy portion (above the boiling energy) of the critical mass curve. In this region the mixing mechanism, which is primarily high energy turbulence, is due to isotropic turbulence if

$$L >> \lambda$$

where L = characteristic linear scale of the mixed system, and

λ = the size of the energy dissipating eddy.

In this case the value of λ can be related to power density from Kolmogoroff turbulence theory[23]

$$\lambda = \frac{\mu^{3/4}}{\rho^{1/2}} \left(\frac{P}{V}\right)^{-1/4} \qquad \text{(B-1)}$$

where μ = viscosity

ρ = density

P = power

V = volume.

A quantity, I_s, called the intensity of segregation can also be defined as[24]

$$I_s = e^{-t/\gamma} \qquad \text{(B-2)}$$

where

$$\gamma = \frac{\lambda^2 \rho}{6\mu}$$

The segregation intensity is also the fraction of one component actually not yet mixed into the other component.

Define a quantity "degree of mixing"

$$f = \frac{m}{M}$$

where m = amount of A mixed with B, and

M = total amount of A in the system.

Then $f = 1 - I_s$

or

$$\frac{m}{M} = 1 - e^{-t/\gamma}. \qquad \text{(B-3)}$$

Equation (B-3) describes the mixedness as a function of time for a batch process.

Now consider a turbulent mixing system in which there is a continuous influx of component A given by dM/dt. Each increment can be thought of as undergoing batch mixing over a time period t. That is

$$dm = dM \left(1 - e^{(t - t')/\gamma}\right) \tag{B-4}$$

where dM is added at time t'. Equation (B-4) must be integrated over all dm to get total mixing as function of time.

$$m = \int \left(1 - e^{-(t-t')/\gamma}\right) dM \tag{B-5}$$

In the special case where M is dropped through a hole from a constant height (the ullage space) it is reasonable to view the flow as constant velocity since the head and opening resistance are approximately constant. Therefore,

$$dM = k_1 dt' \tag{B-6}$$

wnere K_1 is a constant. Since m(o) = 0

$$M = K_1 t'. \tag{B-7}$$

Let $K_2 = 1/\gamma$, then Equation (B-5) becomes

$$m = \int_o^t \left[1 - e^{-K_2(t - t')}\right] K_1 dt' \tag{B-8}$$

after substitution of Equation (B-6). After integration

$$m = K_1 t - \frac{K_1}{K_2}\left(1 - e^{-K_2 t}\right). \tag{B-9}$$

Expand $\left(1 - e^{-K_2 t}\right)$ in a series:

$$1 - e^{-K_2 t} = K_2 t - \frac{K_2^2 t^2}{2!} + \frac{K_2^3 t^3}{3!} - \frac{K_2^4 t^4}{4!} \cdots\cdots$$

then

$$m = \frac{K_1 K_2 t^2}{2!} - \frac{K_1 K_2^2 t^3}{3!} + \frac{K_1 K_2^3 t^4}{4!} - \cdots\cdots$$

for small t

$$m \approx \frac{K_1 K_2 t^2}{2!} = K_3 t^2 . \qquad \text{(B-10)}$$

Now consider the power input. The system gains energy from the falling fluid and, if there are no appreciable friction losses, the energy is

$$E = Mgx$$

where x = ullage space height.

Power is

$$\frac{dE}{dt} = \frac{dM}{dt}\left(gx\right)$$

since g,x are constants.

Since $\frac{dM}{dt} = K_1$ = a constant

then $\frac{dE}{dt} = K_1 gx =$ <u>a constant</u> (B-11)

and the coefficient K_2 is a constant given by

$$K_2 = \frac{6\rho^2 K_1 gx}{\mu^{5/2} V^{1/2}} . \qquad \text{(B-12)}$$

If

$$E = Mgx = K_1 tgx = K_4 t$$

then

$$m = \frac{K_3 E^2}{K_4^2}$$

or

$$m = K_5 E^2. \qquad \text{(B-13)}$$

The validity of the approximation in Equation (B-10) was tested numerically. Typical data in the Farber studies[1] gives mixing times of about 1 sec with yields corresponding to 3000 lb in a 25,000-lb system. If 25,000 lb are added in 1 sec, then $K_1 = 25{,}000$. K_2 can then be estimated from Equation (B-10) by trial and error; in this case $K_2 = 0.26$. Using K_1, K_2 as calculated, Table B-1 was generated. For these values of K_1 and K_2 (which are of the order of magnitude expected) the approximation using one term is very good up to 1 or 2 sec. At most, the approximation is conservative in that larger mixed masses are predicted than are calculated by the exact equation.

TABLE B-1. Comparison of Exact Expression [Equation (B-9)] with Series Approximation

Time, sec	The Mass Mixed (M), lb			
	Exact	1 Term	2 Terms	3 Terms
0.1	32.2	32.5	32.2	32.2
0.2	127.8	130.0	127.7	127.8
0.3	285.0	292.5	284.9	285.0
0.4	502.4	520.0	502.0	502.4
0.5	778.4	812.5	777.3	778.4
0.6	1111.5	1170.0	1109.2	1111.5
0.7	1500.1	1592.5	1495.9	1500.3
0.8	1943.0	2080.0	1935.8	1943.3
0.9	2438.6	2632.5	2427.2	2439.2
1.0	2985.7	3250.0	2968.3	2986.6
2	11011.6	13000.0	10746.7	11039.6
5	55051.1	81250.0	46041.7	57484.4

APPENDIX C

QUENCHING DISTANCE IN DIELECTRICS

Quenching distances discussed in this report are values measured by experiment using metal electrodes. The values are a measure of the greatest wall distance for which wall dissipation of energy or ions can inhibit combustion. A quenching distance so measured is approximately the electrode spacing for which spark energy needed for ignition is smallest. For electrode spacing closer than the quenching distance, wall scavenging of ions and energy makes a more energetic pulse necessary to start combustion.

This study considers ignition by discharges in a dielectric environment, e.g., between dielectric liquid droplets or across bubbles in dielectric liquid. The dielectric should be less effective in suppressing ignition than the metal electrodes for two reasons:

1) Ions are less strongly attracted to the dielectric wall than to metal.

2) The lower thermal conductivity of the dielectric wall results in slower conductive heat dissipation of energy deposited on the surface by radiation, and more re-radiation into the reaction region.

The ion dissipation with low wall distances may occur by the following sequence of events. Following a discharge, ions and electrons are both accelerated toward walls by electrical image forces. Electrons arrive in significant numbers first because of their more rapid acceleration. Following a loss of space charge neutrality, however, ions deposit rapidly because of the stronger collective field force (for short distances to walls). The quenching distance is on the order of the distance cleared of reacting ions in the mean ion reaction time in the combustion process.

A particle of charge q a distance s from a metal wall experiences an image force from induced surface charge given (in rationalized MKS units) by

$$F_s^M = - \frac{1}{4\pi\varepsilon_o} \frac{q^2}{(2s)^2} \qquad \text{(C-1)}$$

The corresponding force from induced polarization of a dielectric wall distance s from the particle is

$$F_s^D = - \frac{1}{4\pi\varepsilon_o} \frac{K-1}{K+1} \frac{q^2}{(2s)^2} \qquad \text{(C-2)}$$

where K is wall dielectric constant. The negative sign in Equations (C-1) and (C-2) comes from measuring distance s positive from wall while the force is directed toward the wall. Neglecting collisional damping and forces from other particles, the particle will be accelerated toward the wall according to

$$m \frac{d^2s}{dt^2} = - \frac{c}{s^2} \qquad \text{(C-3)}$$

where c is a product of factors in E-1 or E-2.

Multiplying Equation E-3 by ds/dt gives

$$m \frac{d^2s}{dt^2} \frac{ds}{dt} = - \frac{c}{s^2} \frac{ds}{dt}$$

or

$$\frac{1}{2} m \frac{d}{dt} \left(\frac{ds}{dt}\right)^2 = c \frac{d}{dt} \left(\frac{1}{s}\right) \qquad \text{(C-4)}$$

Integrating Equation (C-4) from time t=o at which ds/dt is zero and s is s_o to a later time t gives

$$\frac{1}{2} m \left(\frac{ds}{dt}\right)^2 = c\left(\frac{1}{s} - \frac{1}{s_o}\right) . \qquad \text{(C-5)}$$

Taking the square root (and noting ds/dt is negative) and rearranging gives

$$\frac{ds}{\left(\frac{1}{s} - \frac{1}{s_o}\right)^{1/2}} = - \left(\frac{2c}{m}\right)^{1/2} dt. \qquad \text{(C-6)}$$

Note that

$$\frac{ds}{\left(\frac{1}{s} - \frac{1}{s_o}\right)^{1/2}} = \frac{s_o s}{\left(s_o^2 s - s_o s^2\right)^{1/2}} ds \qquad \text{(C-7)}$$

and integrate Equation (C-6) from position s_o at time t=o to position s=o, i.e., hitting wall at time t=T:

$$s_o \left[\frac{\left(s_o^2 s - s_o s^2\right)^{1/2}}{-s_o} + \frac{s_o^2}{2s_o} \frac{1}{\sqrt{s_o}} \sin^{-1} \left(\frac{2s_o s - s_o^2}{s_o^2} \right) \right]_{s=s_o}^{s=o}$$

$$= - \left(\frac{2c}{m}\right)^{1/2} t \Big|_{t=o}^{t=T} \qquad \text{(C-8)}$$

or

$$- \frac{\pi}{2} s_o^{3/2} = - \left(\frac{2c}{m}\right)^{1/2} T. \qquad \text{(C-9)}$$

Isolating initial distance s_o in Equation (C-9) gives

$$s_o = \left(\frac{2}{\pi}\right)^{2/3} \left(\frac{2c}{m}\right)^{1/3} T^{2/3}. \qquad \text{(C-10)}$$

The quenching distance should be on the order of the distance from the wall cleared of ions in a mean ion reaction time. Setting T to the mean ion reaction time on the right hand side of Equation (C-10) should give an approximate quenching distance on the right hand side. We assume that the migration time to the wall of the faster charge species sets the range of quenching. The value of c is different for the metal and the dielectric. Hence from Equation (C-10)

$$\frac{s_o^D}{s_o^M} = \left(\frac{c^D}{c^M}\right)^{1/3} = \left(\frac{K-1}{K+1}\right)^{1/3}. \qquad \text{(C-11)}$$

For dielectric constants K in the range 1.25 to 1.5, the quenching distance by (C-11) should be 0.5 to 0.6 of those for metal.

The foregoing development made no mention of Debye-Hückel screening in the interaction of charges with walls. At the threshold for ignition, the free electron number density should be quite low, and hence the screening distance should be long. The thermal ignition temperature for hydrogen-oxygen mixtures is found to be about 585°C. The Saha equation[25] predicts a low level of thermal ionization at this temperature.

APPENDIX D

CONTACT POTENTIAL FUNDAMENTALS

Each homogeneous object has its characteristic Fermi level which is a function of temperature. The Fermi energy level is the electron energy level above which the probability of occupation of an electron state is less than 50% and below which the probability of occupation is greater than 50%. Specifically, the probability of occupation of an electron state of energy ε is

$$f(\varepsilon, T) = \frac{1}{1 + \exp\left[(\varepsilon-\mu)/kT\right]} \qquad \text{(D-1)}$$

where μ is the "chemical potential" of an electron or the Fermi energy level. The reference point of energy must be the same for both ε and μ. The form for f says that electron states of energy ε much less than μ for which

$$\frac{\varepsilon-\mu}{kT} << -1 \qquad \text{(D-2)}$$

are filled with a probability only slightly less than one. Electron states of energy greater than μ for which

$$\frac{\varepsilon-\mu}{kT} >> 1 \qquad \text{(D-3)}$$

will have a probability much less than one of being occupied.

When two dissimilar objects of homogeneous material are brought into contact, electrons tend to flow so that states of equal energy (relative to the same reference point of energy) have the same probability of being filled in both objects. To see this, consider two metals at temperature T whose electron energy state occupancy is shown in Figure D-1. The electrons in Material 1 see a potential well tending to bind them within the metal. The most tightly bound electrons of the conduction band have an energy ε_{B1} relative to the energy of a distant isolated electron in vacuum. Typically, ε_{B1} (binding energy) will be a negative energy of the order of 10 eV. The conduction electrons in Metal 1 will occupy states which have the energy ε_{B1} plus varying amounts of kinetic energy up to a kinetic energy of approximately ε_{KF1} (kinetic energy at the Fermi level of Material 1). The transition from occupied to unoccupied states occurs in a region of width $\sim kT$ about this value. The Fermi level for isolated Material 1 we give relative to that of an isolated distance electron at rest in vacuum as

$$\mu_1 = \varepsilon_{B1} + \varepsilon_{KF1}. \qquad \text{(D-4)}$$

Note that $-\mu_1$ is the energy needed to remove the most energetic electrons from highly occupied states into vacuum from the neutral metal; note also that our reference point for Fermi energy may differ from that used elsewhere.

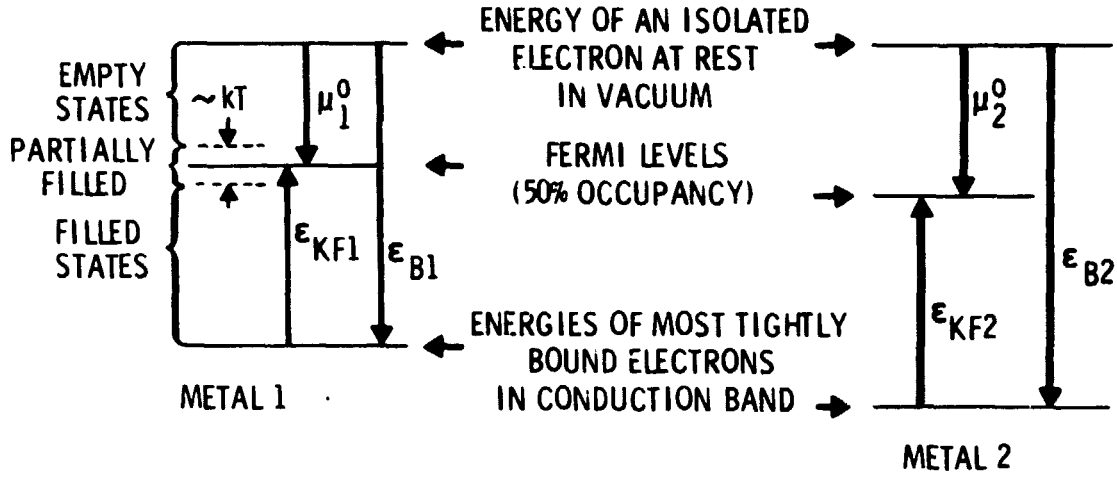

FIGURE D-1. Energy Level Schematic for Two Isolated Neutral Pure Metals, (Note that we measure energies positive upward, so ε_{B1}, ε_{B2}, μ_1, and μ_2 are negative numbers.)

When the metals from Figure D-1 are brought into contact, electrons will initially flow from Metal 1 to Metal 2 (because $\mu_1 > \mu_2$). Only an infinitesimal fraction of the electrons need to flow, however, to create an electric field which stops the flow. The well depths of the two metals will have been shifted by the electrostatic contributions $q_e V_1$ and $q_e V_2$, respectively, when equilibrium is established. Here, q_e is the charge on an electron. The equilibrium situation for the bulk materials is shown in Figure D-2. The condition for no net electron flow between the two media is

$$\mu_1^0 + q_e V_1 = \mu_2^0 + q_e V_2. \qquad \text{(D-5)}$$

Here, the superscript zero on μ_1^0 and μ_2^0 merely indicates that it does not include the electrostatic potential contribution which we have included in our definition of μ. For an inhomogeneous medium at uniform temperature we are led to postulate an electric current density

$$\underline{J} = -\sigma \nabla \left(\frac{\underline{\mu}^0}{q_e} + V\right) \qquad \text{(D-6)}$$

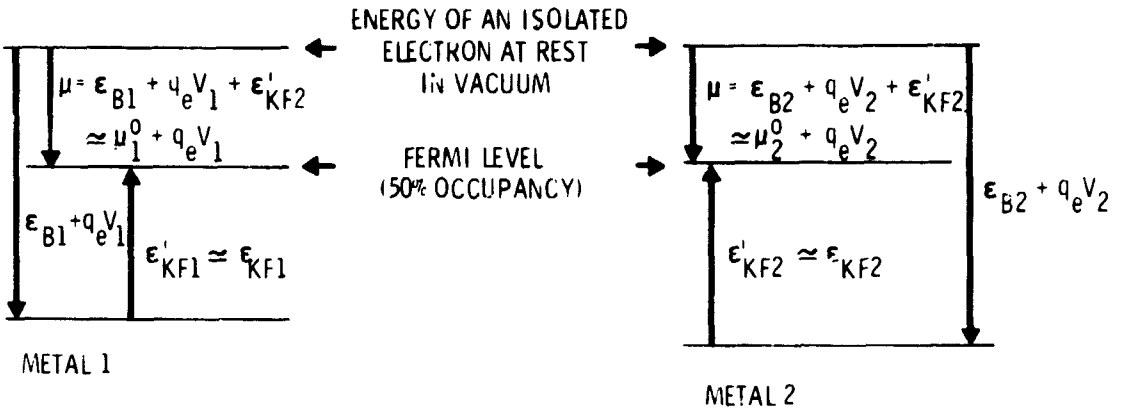

FIGURE D-2. Energy Level Schematic for Two Pieces of Dissimilar Metals Brought into Contact

in the absence of magnetic field. This reduces to the familiar $\underline{J} = -\sigma \nabla V$ or $\underline{J} = \sigma \underline{E}$ with conductivity σ for a homogeneous medium. This is in agreement with Landau and Lifshitz.[26] With nonuniform temperature, a current contribution proportional to temperature gradient must be added:

$$\underline{J} = \sigma \left(- \nabla \left(\frac{\mu^0}{q_e} + V \right) - \alpha \nabla T \right). \qquad \text{(D-7)}$$

For a contact between dissimilar semiconductors or good resistors, similar considerations apply. A charge transfer occurs on contact to equalize the Fermi levels in the two materials, although Fermi levels will for resistors or semiconductors typically be mathematical energies only [in the Fermi-Dirac distribution, Equation (D-1)], not energies of actual allowed electron states. Also the approach to equilibrium will be very slow compared to that in metals.

The potential difference $V_2 - V_1$ between the dissimilar materials comes physically from a charge distribution at the interface. This interface charge distribution for good conductors is very thin, and is frequently considered as a dipole layer. For a germanium junction with 10^{15} donor atoms per cubic centimeter in contact with a metal, the space charge region is estimated to be 10^{-4} cm thick[27] at room temperature. For electrolytes as well as semiconductors, the thickness of the space charge region varies with the inverse square root of the number density

of current carriers. This finite thickness of the space charge region (particularly at cryogenic temperatures) for low temperature materials with an extremely low density of charge carriers gives an opportunity for pronounced charging effects in vaporization induced bubbling and frothing. It should be noted that the slow relaxation time in highly resistive liquids or vapors implies that the charge separation may occur only if the vapor bubbles have traveled through the medium long enough for charge separation to have occurred.

REFERENCES

1. E. A. Farber, J. H. Smith, and E. H. Watts, "Final Report, Prediction of Explosive Yield and Other Characteristics of Liquid Rocket Propellant Explosions," Contract No. NAS10-1255, June 30, 1973.

2. Project PYRO Final Reports, "Liquid Propellant Explosive Hazards," vol. 1, 2, and 3, December 1968. AFRPL-TR-68-92; URS 652-35. Prepared under contract AF04 (611) 10739 for Air Force Rocket Propulsion Laboratory, Air Force Systems Command, USAF, Edwards, CA.

3. J. B. Gayle, "Investigation of S-IV All Systems Vehicle Explosion," MSC, Huntsville, AL, NASA TMX-53059, April 27, 1964.

4. E. A. Farber et al., "Electrostatic Charge Generation and Autoignition Results of Liquid Propellant Experiments," Report No. X, NAS10-1255, October 1972.

5. A. D. Little, Inc., Interim Report on an Investigation of Hazards Associated with Liquid Hydrogen Storage and Use, Contract No. AF 18(600)-1687 C-61092, January 15, 1959.

6. H. R. Kruyt, Colloid Science, vol. 1, Elsevier Publishing Co., Amsterdam, 1952. (See Chapter 5 for extensive summaries of development.)

7. H. B. Bull, Kolloid-Z., no. 66, p. 20, 1934.

8. H. R. Kruyt and P. C. Van Der Willegen, Kolloid-Z., no. 45, p. 307, 1928.

9. H. R. Kruyt, Colloid Science, vol. 1, Elsevier Publishing Company, Amsterdam, 1952.

10. Herman Schlicting, Boundary Layer Theory, McGraw-Hill, New York, 4th ed., p. 25, 1960.

11. L. Cassutt, D. Biron, and B. Vonnegut, "Electrostatic Hazards Associated with the Transfer and Storage of Liquid Hydrogen," Adv. Cryogenic Eng., vol. 7, 1961.

12. H. R. Kruyt, Colloid Science, vol. 1, Elsevier Publishing Company, Amsterdam, p. 228, 1952.

13. R. B. Scott, W. H. Denton, and M. Nicholls (eds.), Technology and Uses of Liquid Hydrogen, Pergaman Press, New York, (numbers taken from Figure 2, p. 364), pp. 363-364, 1964.

14. W. R. Harper, "Liquids Giving No Electrification by Bubbling." Static Electrification, A symposium held by The Institute of Physics in London, March 1953. British Journal of Applied Physics, Supplement No. 2, 1953.

15. Charles Kittel, Introduction to Solid State Physics, Third Edition, John Wiley and Sons, Inc., New York, NY, 1966. See Chapter 10.

16. G. B. Yates, A. R. Perl, J. F. Loos, and R. J. Sergeant, "Spark Ignition Parameters of Cryogenic Hydrogen in Oxygen and Nitrogen Mixtures," Paper G-2, Proc. Cryo. Eng. Conf., no. 10, part I, p. 265, 1964.

17. L. C. Northcliffe and R. F. Schilling, "Range and Stopping Power Tables for Heavy Ions," Nuclear Data Tables A, vol. 7, no. 3-4, January 1970.

18. R. B. Scott, Cryogenic Engineering, D. Van Nostrand Co., Inc., New York, p. 305, 1959.

19. Farkas and Sachsse, Z. Physik. Chem., B23, vol. 1, p. 19, 1933.

20. S. J. D. Van Stralen, Int. J. Heat and Mass Trans., 9, (12), pp. 1463-70, 1966.

21. R. H. Fowler and E. A. Guggenheim, Statistical Thermodynamics, Macmillan Company, New York, NY, pp. 138-139, 1949.

22. E. Kamke, Differentialgleichungen Lösungsmethoden und Lösungen, Chelsea Publishing Company, New York, NY, p. 27, 1948.

23. P. H. Calderbank, "Mass Transfer," Mixing Vol. II, Uhl and Gray (eds.), Academic Press, New York, p. 20, 1967.

24. R. S. Brodkey, "Fluid Motion and Mixing," Mixing Vol. I, Uhl and Gray (eds.), Academic Press, New York, p. 71, 1967.

25. Landau and Lifshitz, Statistical Physics, Addison-Wesley, Reading, MA, vol. 106, p. 323, 1969.

26. Landau and Lifshitz, Electrodynamics of Continuous Media, Addison-Wesley, Reading, MA, p. 105, 1960.

27. E. V. Condon and Hugh Odishaw, ed., Handbook of Physics, McGraw-Hill, New York, 1958. Section 8, Chapter 4, "Flow of Electrons and Holes in Semiconductors," John Bardeen.